Supporting Information

Polypyridyl Iron Complex as a Hole Transporting Material for Formamidinium Lead Bromide Perovskite Solar Cells

Muhammad K. Kashif,[†,+] *Iacopo Benesperi,*[‡,+] *Rebecca A. Milhuisen,*[†,§] *Steffen Meyer,*[‡] *Jack Hellerstedt,*[‖,⊥,#] *David Zee,*[▽,○] *Noel W. Duffy,*[◆] *Barry Halstead,*[◆] *Michael S. Fuhrer,*[‖,⊥,#] *John Cashion,*[‖] *Yi-Bing Cheng,*[†] *Leone Spiccia,*[‡,¶] *Alexandr N. Simonov,*[*,‡,¶] *and Udo Bach*[*,§,◆,&,$]

[†]Department of Materials Science and Engineering, 20 Research Way, Monash University, Victoria 3800, Australia

[‡]School of Chemistry, 17 Rainforest walk, Monash University, Victoria 3800, Australia

[§]ARC Centre of Excellence in Exciton Science, Monash University, Victoria 3800, Australia

[‖]School of Physics and Astronomy, 19 Rainforest Walk, Monash University, Victoria 3800, Australia

[⊥]Monash Centre for Atomically Thin Materials, Monash University, Victoria 3800, Australia

[#]Center for Nanophysics and Advanced Materials, University of Maryland, College Park, Maryland 20742-4111, USA

[▽]Department of Chemistry, University of California, Berkeley, 420 Latimer Hall, Berkeley, California 94720, USA

[○]Materials Sciences Division, Lawrence Berkeley National Laboratory, 1 Cyclotron Road, Berkeley, California 94720, USA

[◆]CSIRO, Research Way, Clayton, Victoria 3168, Australia

[¶]ARC Centre of Excellence for Electromaterials Science, Monash University, Victoria 3800, Australia

[&]Melbourne Centre for Nanofabrication, 151 Wellington Road, Clayton, Victoria 3168, Australia

[$]Department of Chemical Engineering, Monash University, Victoria 3800, Australia

ABSTRACT: An efficient hole transporting material (HTM) is indispensable for high-performing perovskite solar cells (PSC), which have recently emerged as a breakthrough photovoltaic technology. Here, we demonstrate the capacity of the transition metal complex (6,6′-bis(1,1-di(pyridin-2-yl)ethyl)-2,2′-bipyridine)-iron(II/III) trifluoromethanesulfonate ([Fe(bpyPY4)](OTf)$_{2+x}$) to act as an additive-free, solution-processable HTM in PSCs based on the formamidinium lead bromide absorber. State-of-the-art physical methods have been employed to characterize [Fe(bpyPY4)](OTf)$_{2+x}$ and in particular to demonstrate its significantly higher conductivity compared to the conventional HTM spiro-OMeTAD. A maximum power conversion efficiency of 2.2% was obtained for a device employing [Fe(bpyPY4)](OTf)$_{2+x}$, which is the first evidence of the applicability as HTM in PSC of a solid material in which conductivity is provided by a redox transformation of a transition metal.

Table of contents

Experimental methods

Materials

Unless otherwise specified, all materials were purchased from either Alfa Aesar or Sigma-Aldrich and used as received. Spiro-OMeTAD (2,2',7,7'-tetrakis-(*N*,*N*-di-4-methoxyphenylamino)-9,9'-spirobifluorene) was purchased from Luminescence Technology Corp. (Lumtec). Fluorine-doped tin oxide (FTO) glass TEC8 (sheet resistance 8 $\Omega\ \square^{-1}$) was purchased from Dyesol. Interdigitated array microelectrodes were purchased from BAS-ALS, Japan.

Synthesis of 6,6'-bis(1,1-di(pyridin-2-yl)ethyl)-2,2'-bipyridine (bpyPY4)

The ligand bpyPY4 was synthesized according to a method reported in the literature.[S1] In a round-bottomed flask under nitrogen atmosphere, 2,2'-(ethane-1,1-diyl)dipyridine (2.28 g, 12.4 mmol, 3 eq) was added to 90 mL of dry tetrahydrofuran (THF). The solution was cooled down to −78 °C (acetone/dry ice). Once the temperature was reached, *n*-butyllithium (2.5 M in hexane, 5 mL, 12.5 mmol, 3 eq) was added dropwise and the solution was stirred for 30 min. A solution of 6,6'-dibromo-2,2'-bipyridine (1.30 g, 4.14 mmol, 1 eq) in 45 mL of dry THF (prepared under nitrogen atmosphere, gentle heating may be required for full dissolution) was subsequently added, and the cooling bath removed. The solution was stirred for 1 h, then refluxed for 36 h while keeping the nitrogen atmosphere. After cooling to room temperature, the reaction was quenched with 60 mL of water. The organic and aqueous phases were separated and the aqueous phase was washed three times with dichloromethane for a total amount of 60 mL. The combined organic phases were dried with $MgSO_4$ and the solvent removed with rotary evaporation. The crude product was suspended in ethyl acetate and kept in an ultrasonic bath for 1.5 h. After decanting, ethyl acetate was pipetted out and replaced with a fresh portion, and the sonication was repeated. Afterwards, the slightly beige solid was filtered and used as is. Yield: 1.46 g (68%). ^{1}H NMR (400 MHz, $CDCl_3$): δ = 8.57 (dq, *J* = 1 Hz, 4.8 Hz, 4H), 8.01 (dd, *J* = 0.8 Hz, 7.8 Hz, 2H), 7.60-7.52 (m, 6H), 7.12-7.07 (m, 10H), 2.39 (s, 6H).

Synthesis of [Fe(bpyPY4)](OTf)$_2$

Inside a glove-box, bpyPY4 (0.30 g, 0.576 mmol, 1 eq) was suspended in 5 mL of CH_3CN inside a vial. In a separate vial, $Fe(OTf)_2$ (0.20 g, 0.565 mmol, 1 eq) was dissolved in 6 mL of CH_3CN. The $Fe(OTf)_2$ solution was added dropwise to the bpyPY4 suspension while stirring at 60 °C. After addition, the mixture was allowed to stir for 30 min and then filtered through a 0.45 μm PTFE membrane syringe filter to remove the excess of undissolved bpyPY4. The vial containing the metal complex solution was placed in a capped Schott bottle containing diethyl ether and the metal complex was obtained through recrystallization *via* solvent diffusion over two weeks. The crystals were recovered, washed with $(C_2H_5)_2O$ and dissolved again in a minimum amount of CH_3CN. The solution was placed in a Schott bottle again for a second recrystallization in a similar fashion. The obtained crystals were blood-red in color. Yield: 0.34 g (69%). ^{1}H NMR (400 MHz, DMSO-d6): δ = 8.52 (d, *J* = 7 Hz, 2H), 8.45 (d, *J* = 8 Hz, 2H), 8.32 (d, *J* = 7.4 Hz, 2H) 8.25-8.18 (m, 4H), 7.95-7.87 (m, 4H), 7.82 (dd, *J* = 1.2 Hz, 5.1 Hz, 2H), 7.28 (ddd, *J* = 1 Hz, 7.6 Hz, 6 Hz, 2H), 7.21 (dd, *J* = 1.4 Hz, 6.8 Hz, 2H), 6.98 (ddd, *J* = 1.4 Hz, 7.1 Hz, 5.2 Hz, 2H), 2.89 (s, 6H). HR-MS (ESI): *m/z* calcd for $[Fe(bpyPY4)]^{2+}$: 228.0857, found: 228.0849; calcd for $[Fe(bpyPY4)](OTf)^+$: 725.1240, found: 725.1220; calcd for OTf^-: 148.9526, found: 148.9529. Elem. anal. calcd for $C_{36}H_{28}F_6FeN_6O_6S_2$: C, 49.44; H, 3.23; Fe, 6.39; N, 9.61; S, 7.33. Found: C, 49.65; H, 3.18; Fe, 6.40; N, 9.74; S, 7.35.

Synthesis of [Fe(bpyPY4)](OTf)$_3$

The synthetic procedure for the Fe(III) complex is equivalent to the one for [Fe(bpyPY4)](OTf)$_2$. In this case, the initial quantity of Fe(OTf)$_3$ was 0.78 g (0.760 mmol, 1 eq) and the initial quantity of bpyPY4 was 0.40 g (0.768 mmol, 1 eq). The obtained crystals were dark red/brown in color. Yield: 0.75 g (95%). Elem. anal. calcd for $C_{37}H_{28}F_9FeN_6O_9S_3$: C, 43.41; H, 2.76; Fe, 5.46; N, 8.21; S, 9.40. Found: C, 44.01; H, 2.89; Fe, 5.34; N, 9.15; S, 8.73. Given that Mössbauer spectroscopy identified a 7.8 atom % Fe(II) impurity in the synthesized compound, it is referred to as [Fe(bpyPY4)](OTf)$_{2.9}$ hereinafter.

Synthesis of formamidinium bromide (FABr)

In a 250 mL beaker, formamidinium acetate (18.41 g, 177 mmol, 1 eq) was dissolved in a 48% w/w solution of HBr in water (40 mL, 354 mmol, 2 eq). The solution was stirred at 50 °C for 1 h and the solvent was subsequently removed at 100 °C under a nitrogen stream to facilitate evaporation. The obtained solid was washed with diethyl ether and recrystallized twice from ethanol. The purification process yielded white crystals. The obtained powder was kept at 80 °C under high vacuum overnight to ensure complete dryness and then handled under inert atmosphere. Yield: 11.54 g (52%). ^{1}H NMR (400 MHz, MeOD-d4): δ = 7.86 (s, 1H).

Conductivity measurements

Interdigitated array (IDA) microelectrodes were comprised of 65 gold electrode pairs spaced 10 μm apart on a quartz substrate. Each electrode finger was 5 μm wide, 2 mm long and 90 nm thick. A non-conducting passivation layer masked most of the substrate, exposing the 2 × 2 mm area of the IDA gold electrode pairs. Prior to use, IDA electrodes were thoroughly washed with acetonitrile and dried under a stream of nitrogen.

Inside a glove-box, equimolar solutions of [Fe(bpyPY4)](OTf)$_2$ and [Fe(bpyPY4)](OTf)$_{2.9}$ were prepared by dissolving [Fe(bpyPY4)](OTf)$_2$ (43.7 mg, 50 mM) and [Fe(bpyPY4)](OTf)$_{2.9}$ (51.2 mg, 50 mM) in acetonitrile (1 mL). Solutions of various compositions (from Fe^{2+} to Fe^{3+}) were prepared by mixing the required amounts of the aforementioned solutions. For comparison with a standard hole-conducting material, a 10% oxidized spiro-OMeTAD solution in chlorobenzene was prepared following a previously described method.[S2] Briefly, spiro-OMeTAD dissolved in dichloromethane was oxidized by reaction with an equimolar amount of Ag(OTf) to give spiro-OMeTAD(OTf) and Ag^0. Silver was removed by filtration and spiro-OMeTAD(OTf) was purified *via* precipitation from the solution with diethyl ether. 10 mol % of spiro-OMeTAD(OTf) was added to the spiro-OMeTAD solution used for the experiments. Solutions were drop-cast onto the electrode so that the film was covering both the interdigitated area and the surrounding passivation layer. IDAs coated with such thin films were then allowed to dry under nitrogen atmosphere inside the glove-box.

A Bio-Logic VSP potentiostat was used to record current-voltage characteristics of the two-probe IDA electrodes. The potential was cycled between −0.5 and +0.5 V at a scan rate of 0.10 V s^{-1}. Room temperature conductivity measurements were undertaken inside a glove-box. Conductivity measurements over the temperature range 10-300 K were performed using a physical property measurement system that uses liquid helium. Thin films on IDA electrodes were exposed for a very short time to air upon transferring and loading into the sample chamber of the cryostat. The sample chamber was purged with helium gas and sealed at atmospheric pressure, and measurements were undertaken starting at 300 K and cooling down in 10 or 5 K intervals.

The conductivities (σ) of the thin films were calculated from the slope of the acquired current-voltage curves by applying the relationship $\sigma = S(d/((2n-1)lh))$ [S m^{-1}] (where S is the slope of the linear fit to the experimental I-V data, d is the electrode spacing, n is the number of electrode pairs, l is the electrode length and h is the film thickness). The film thickness was measured using an optical profilometer on scratches engraved along both sides of the electrode area after acquiring the current-voltage data.

Solar cell preparation

Glass covered with fluorine-doped tin(IV) oxide (FTO) was patterned using a laser engraver (Universal Laser Systems, VLS3.50) and subsequently washed in three steps with a 1 vol % solution of Hellmanex in water, pure water and 96 vol % ethanol, each time under sonication (Elma, Elmasonic S300H) at 50 °C for 20 min. After the last cleaning step, the FTO substrates were dried under an air stream. A compact TiO_2 blocking layer (c-TiO_2) was deposited onto the FTO surface by spray pyrolysis, employing 2.8 mL of a titanium diisopropoxide bis(acetylacetonate) solution in isopropanol (1:9 vol.) and a substrate temperature of 475 °C. Prior to perovskite deposition, the FTO|c-TiO_2 substrates were further cleaned by ozone plasma for 10 min (Harrick Plasma, PDC-002; plasma intensity set to "high"; air pressure inside the chamber *ca* 1100 mTorr).

All further procedures were carried out in a glove-box under a high-purity nitrogen atmosphere with less than 0.1 ppm oxygen and water. The perovskite precursor solution (30 weight %) was prepared by dissolving FABr (52.3 mg) and $PbBr_2$ (153.6 mg) in *N*,*N*-dimethylformamide (470 µL). After dissolution, a 47% w/w solution of HBr in water was added (23.4 µL). The spiro-OMeTAD solution was prepared by dissolving spiro-OMeTAD (20.6 mg) in chlorobenzene (250 µL). The [Fe(bpyPY4)](OTf)$_{2.5}$ solution was prepared by dissolving [Fe(bpyPY4)](OTf)$_2$ (21.9 mg) and [Fe(bpyPY4)](OTf)$_{2.9}$ (25.6 mg) in nitromethane (1 mL), giving a Fe^{II}:Fe^{III} ratio of approximately 1:1. In the preliminary experiments, 4-*tert*-butylpyridine and lithium bis(trifluoromethanesulfonyl)imide were introduced into the HTM solutions. However, further studies have indicated that the best performance of the solar cells based on both spiro-OMeTAD and [Fe(bpyPY4)](OTf)$_{2+x}$ are achieved with additive-free HTM layers.

A ~1.2 cm^2 perovskite layer was deposited on the FTO|c-TiO_2 substrate by spin-coating 25 µL of the perovskite solution at 4000 rpm for 30 s with an acceleration of 4000 rpm s^{-1}. Upon 3 s of the spinning, a 380 kPa nitrogen flow was applied for 10 s.[S3] The resulting film was annealed on a hotplate at 170 °C for 10 min. After cooling, an HTM layer was deposited by spin-coating either 25 µL of the spiro-OMeTAD solution at 3000 rpm for 30 s with an acceleration of 3000 rpm s^{-1}, or 18 µL of the [Fe(bpyPY4)](OTf)$_{2.5}$ solution at 2000 rpm for 40 s with an acceleration of 200 rpm s^{-1}. As a final step, a 80 nm layer of Au was deposited by thermal evaporation (DDong DD-GCMO3CR; deposition started when vacuum reached 3×10^{-1} Torr; deposition speed: 0.2 Å s^{-1} between 0-50 Å, 1 Å s^{-1} between 50-400 Å, 2.5 Å s^{-1} between 400-800 Å).

Device encapsulation was performed under nitrogen atmosphere (glove-box) by dispensing UV-curable epoxy resin from Lumtec (LT-U001) onto the edges of a cover glass with a recess in the middle (purchased from HanaAMT). The glass was then gently pressed on the solar cell devices before being illuminated under UV light (2.5 mW cm^{-2}, peak intensity at 365 nm) for 12 min.

Characterization

NMR analysis was performed on a Bruker Avance III 400 equipped with an Ultrashield 400 Plus magnet.

High resolution mass spectroscopic analysis was performed on an Agilent 6220 Accurate Mass LC-TOF system with Agilent 1200 Series HPLC. The mass spectrometer was fitted with the Agilent Multimode Source. The reference compound used for reference mass correction was a purine/HP0921 mix. The syringe pump used for injection was a KD Scientific syringe pump running at 600 μL h^{-1}. ESI conditions: 8 L min^{-1} N_2, 325° drying gas temperature; capillary voltage: 3500 V; fragmentor voltage: 160 V.

UV-Vis spectra were recorded on a PerkinElmer Lambda 950 spectrophotometer.

Photoluminescence spectra were recorded on a Horiba Jobin-Yvon FluoroMax-4 with an excitation wavelength of 380 nm and 4.3 nm slit aperture, using internal signal, blank and baseline corrections.

Mössbauer spectra were taken on a standard Wissel spectrometer operating in constant acceleration mode with data collection into 1024 channels. The ^{57}Co in Rh source and the absorber were kept at room temperature. Calibration was carried out using α-iron and all isomer shifts are quoted relative to α-iron at room temperature. The samples were sealed into perspex holders at a loading of 140 mg cm^{-2}. The spectra were least squares fitted to doublets using Voigtian profiles, with corresponding members having the same intensity and linewidth.

X-ray diffraction (XRD) patterns of FTO, lead bromide and perovskite films were recorded on a Philips PW1130 X-ray diffractometer with Cu K_α radiation at 2° min^{-1} with 0.02° resolution. XRD patterns of the $[Fe(bpyPY4)](OTf)_{2.5}$ films were recorded on a Bruker D2 Phaser X-ray diffractometer with Cu K_α radiation (λ = 1.54184 Å) with 0.02° resolution. The drop-cast and spin-coated films were analyzed at 1.2 and 0.2° min^{-1}, respectively.

Photoelectron spectroscopy in air (PESA) measurements were conducted on a Riken Keiki AC-2 photoelectron spectrometer. The error in the ionization energies determined from the PESA measurements on a given sample was ±0.05 eV.

Ultraviolet photoelectron spectroscopy (UPS) analysis was performed using an AXIS Ultra DLD spectrometer (Kratos Analytical Inc., Manchester, UK) with a helium discharge source optimized for He I radiation (21.22 eV), a hemispherical analyzer operating in the fixed analyzer transmission mode and the standard aperture (analysis area > 1 mm^2). The total pressure in the main vacuum chamber during analysis was typically between 10^{-9} and 10^{-8} mbar. Each specimen was analyzed at an emission angle of 0° as measured from the surface normal and samples were biased at −2 V. The bias serves to facilitate the observation of the secondary electron cut-off from the UPS data by separating sample analyzer cut-offs and providing a higher secondary electron yield. Valence band spectra were acquired at a pass energy of 5 eV with a step width of 0.025 eV. The error in the ionization energies determined by UPS was estimated to be ±0.1 eV.

Scanning electron microscopy (SEM) surface profile and cross-section images were recorded using a FEI Magellan 400 FEG microscope. Images were captured using an accelerating potential of 5 kV and a beam current of 6.3 pA. Cross-section samples were prepared by fracturing the complete solar cell devices. Energy dispersive X-ray (EDX) point analyses were performed using a FEI Nova NanoSEM 450 microscope fitted with a Bruker Quantax 400 X-ray analysis system. Analyses were performed using an accelerating potential of 5 kV and a spot size 6 at 20k magnification.

Current-voltage (J-V) characterization of the solar cells was performed using a Photo Emission Tech. model SS50AAA solar simulator with the current-voltage curves measured by a Bio-Logic VSP potentiostat. The intensity of the solar simulator was set using a calibrated silicon reference cell with a KG3 glass filter (PV Measurements, Inc.). The curves were recorded at a scan rate of 0.01 V s^{-1} with a delay of 0.1 s from forward bias to the short circuit condition. Steady state current characterization was performed using the same solar simulator employed for the current-voltage characterization. The device was connected to a BioLogic VSP potentiostat to record the current at a fixed voltage taken from the maximum power point of the *J-V* curve over time every 0.1 s.

Incident photon-to-electron conversion efficiency (IPCE) spectra were measured by dispersing light from a 300 W xenon lamp through a monochromator (Oriel Cornerstone 260). The short-circuit current was recorded using a Keithley 2400 source measure unit. The system was calibrated with a calibrated photodiode (Peccell technologies).

Long-term stability measurements were conducted inside a Vötsch Atlas SC^3 340 environmental chamber equipped with a solar simulator. The chamber temperature was maintained at 25 °C (actual cell temperature was higher due to continuous irradiation) and the relative humidity inside the chamber was 20%. Solar cells were kept under constant 1 sun AM1.5G illumination for 120 h under open circuit condition. *J-V* curves for each cell were measured every 10 minutes. Light intensity fluctuations were monitored through the measurement of a reference Si solar cell and the maximum intensity variation during the experiment was within ±2.5% of the nominal value.

Electrochemical impedance spectroscopic measurements were performed under 27 mW cm^{-2} illumination provided by a 435 nm LED powered by a PP210 potentiostat. Spectra were recorded using a 10 mV perturbation at an applied potential of 400 and 700 mV for the $[Fe(bpyPY4)](OTf)_{2.5}$ and spiro-OMeTAD-based devices, respectively. A Zahner Zennium electrochemical workstation ECW IM6 was used as a frequency response analyzer, and impedance measurements were performed in the 4 MHz to 1 Hz frequency range. Impedance data were analyzed using Zview equivalent circuit modeling software (Scribner).

Results

Single crystal XRD details for $[Fe(bpyPY4)](OTf)_2$ and $[Fe(bpyPY4)](OTf)_3$

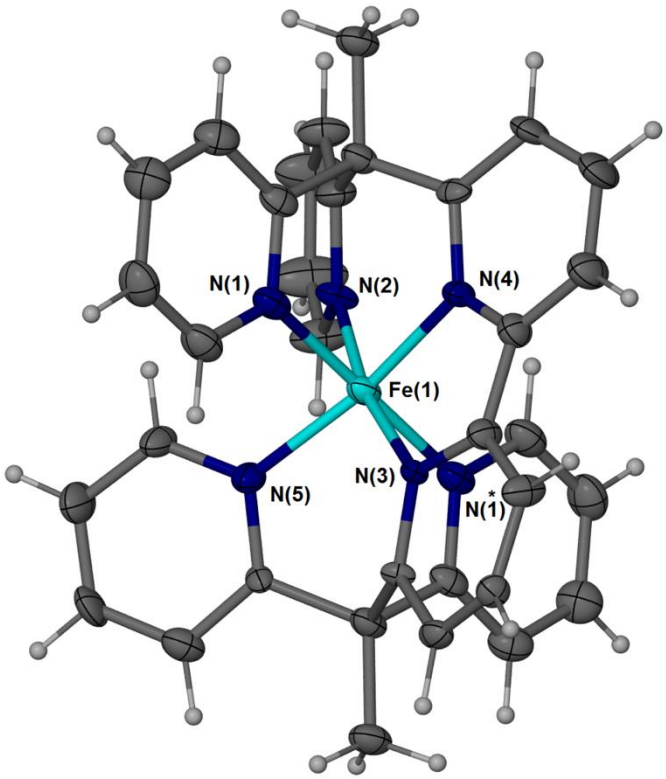

Crystal data for $[Fe(bpyPY4)](OTf)_2$
Crystal composition: $[Fe(bpyPY4)](OTf)_2$
Crystal system, space group: Triclinic, P-1
Unit cell dimensions: a = 8.3101(3) Å α = 114.636(4) deg
b = 10.4017(3) Å β = 95.979(3) deg
c = 11.6371(5) Å γ = 98.975(3) deg

Crystal data for $[Fe(bpyPY4)](OTf)_3$
Crystal composition: $[Fe(bpyPY4)](OTf)_3 \cdot MeCN$
Crystal system, space group: Monoclinic, $P2_1/n$
Unit cell dimensions: a = 18.2511(10) Å α = 90 deg
b = 13.9494(5) Å β = 117.614(7) deg
c = 19.6316(10) Å γ = 90 deg

Figure S1. Structure of $[Fe(bpyPY4)]^{2+}$ with 50% thermal ellipsoids; geometry inferred by single crystal X-ray analysis. Crystal data for $[Fe(bpyPY4)](OTf)_2$ and $[Fe(bpyPY4)](OTf)_3$. The complete data refinements for both $[Fe(bpyPY4)](OTf)_2$ and $[Fe(bpyPY4)](OTf)_3$ are given in the tables at the end of the Supporting Information.

XRD patterns of $[Fe(bpyPY4)](OTf)_{2.5}$ films

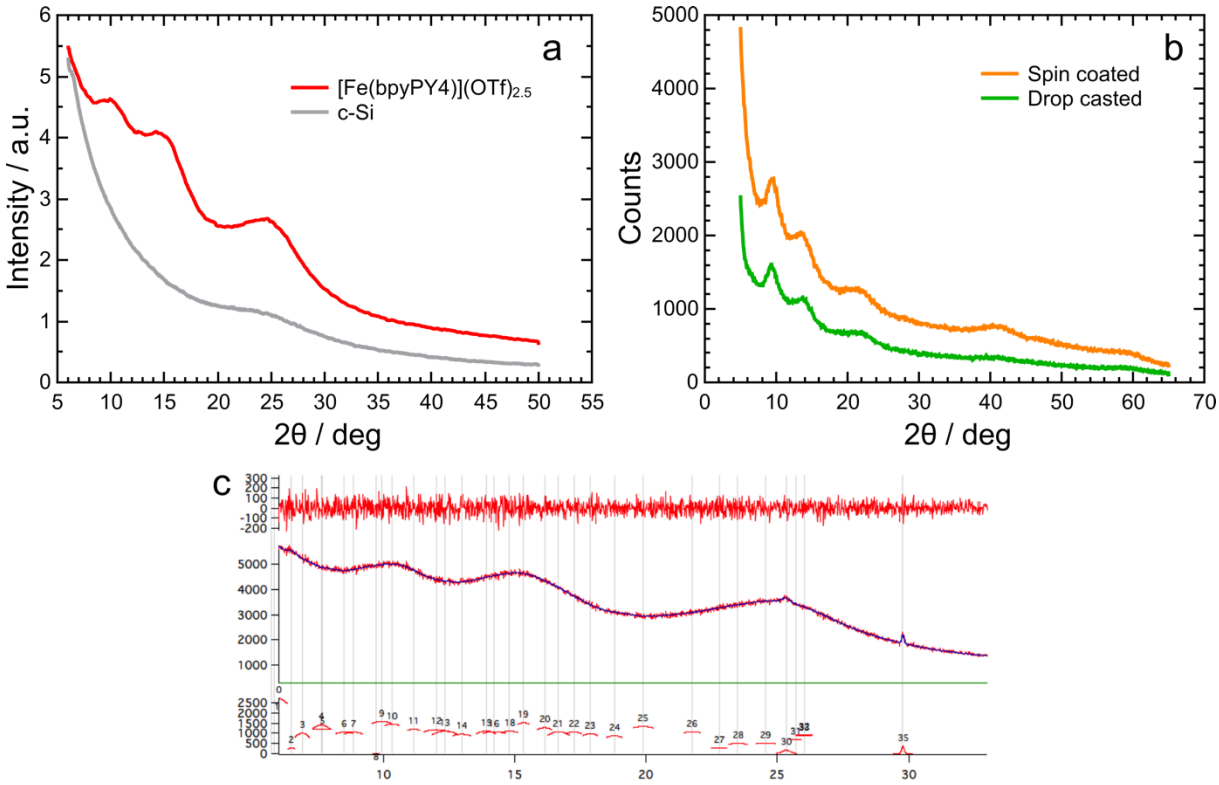

Figure S2. X-ray diffraction analysis of the thin $[Fe(bpyPY4)](OTf)_{2.5}$ films. (a) Grazing angle X-ray diffractogram (GAXRD) of a 0.95 μm thick film spin-coated onto a single crystalline Si substrate (*red*). The *gray* curve shows the diffractogram of an uncoated substrate. (b) XRD patterns of films deposited by drop-casting (*green*) and spin-coating (*orange*). (c) Fitting of the GAXRD pattern from panel **a** using the single-crystal data for $[Fe(bpyPY4)](OTf)_2$ with peak broadening defined by Sherrer equation and crystallite sizes ranging from 30 nm to sub-nanometer scale.

Mössbauer spectroscopy

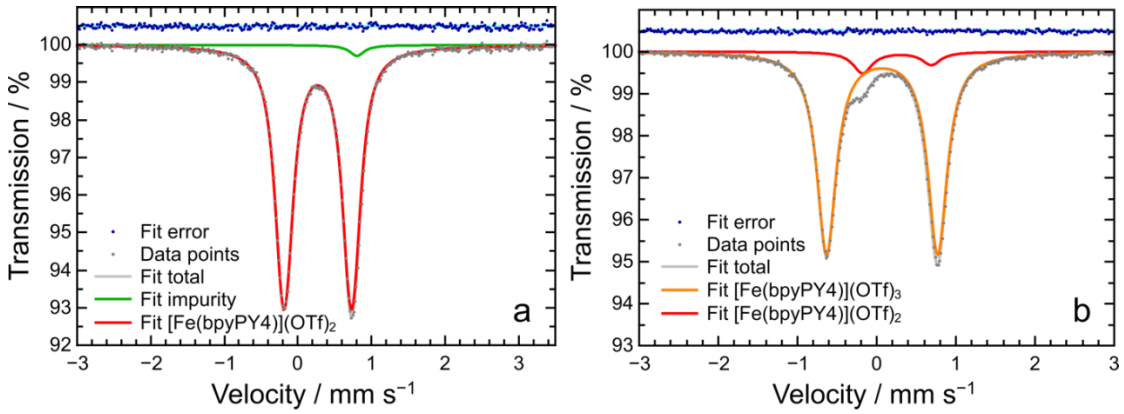

Sample	χ^2	Ferric doublet				Ferrous doublet				
		ö [mm s^{-1}]	Δ [mm s^{-1}]	Γ [mm s^{-1}]	Area [%]	ö [mm s^{-1}]	Δ [mm s^{-1}]	Asym. A(L)/A(R)	Γ [mm s^{-1}]	Area [%]
Fe[bpyPY4](OTf)$_3$	0.504	0.07(1)	1.40(1)	0.31(1)	92.2	0.26(1)	0.86(2)	1.67(7)	0.29(1)	7.8
Fe[bpyPY4](OTf)$_2$	0.675					0.27(1)	0.92(1)		0.31(1)	98.1

Figure S3. Mössbauer spectra of (a) [Fe(bpyPY4)](OTf)$_2$ and (b) [Fe(bpyPY4)](OTf)$_3$ with voigtian fitting of two populations. For both images, the fit error is the difference between the value of the total fitting line and the data point at each velocity value, centered on a line at 100.5% transmission for easiness of plotting. The spectrum of [Fe(bpyPY4)](OTf)$_2$ shows a doublet corresponding to the Fe(II) complex (*red*) and a singlet corresponding to an impurity (1.9 atom %, *green*). The spectrum of [Fe(bpyPY4)](OTf)$_3$ shows a symmetric doublet corresponding to the Fe(III) complex (*orange*) and an asymmetric doublet corresponding to the Fe(II) complex (*red*); the asymmetry is attributed to crystal field effects. The table lists all main parameters for the Fe(II) and Fe(III) doublets in each sample. ö – isomer shift; Δ – quadrupole splitting; Γ – linewidth; Asym. – asymmetry of the doublet given as the ratio of the areas of the left and right peaks; Area – total area of the doublet.

UV-Vis absorbance

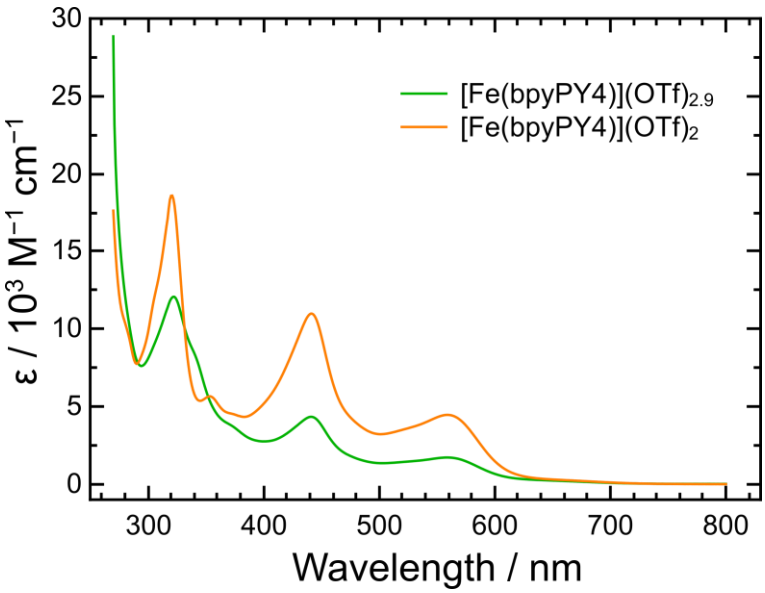

Figure S4. UV-Vis spectra of [Fe(bpyPY4)](OTf)$_2$ (*orange*) and [Fe(bpyPY4)](OTf)$_{2.9}$ (*green*) measured in acetonitrile at room temperature, indicating the molar extinction coefficient.

Conductivity

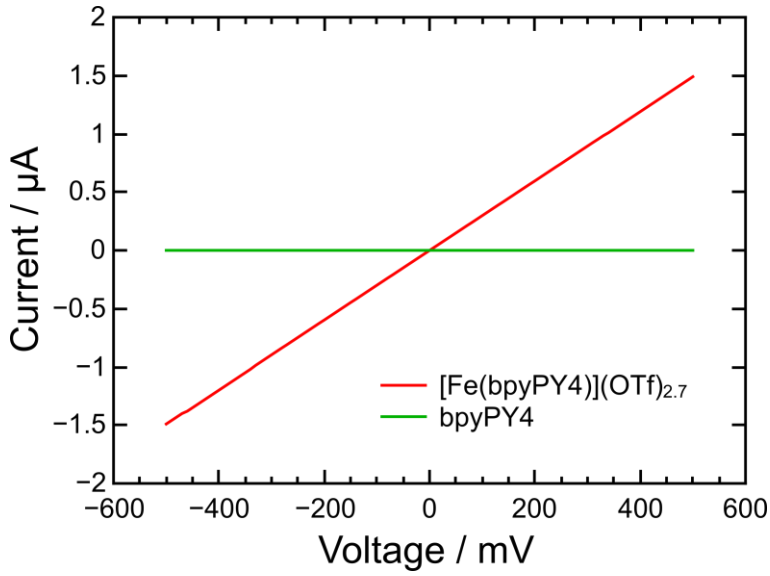

Figure S5. Room temperature current-voltage curve for the [Fe(bpyPY4)](OTf)$_{2.7}$ (*red*) and bpyPY4 (*green*) thin films drop-cast onto an IDA electrode.

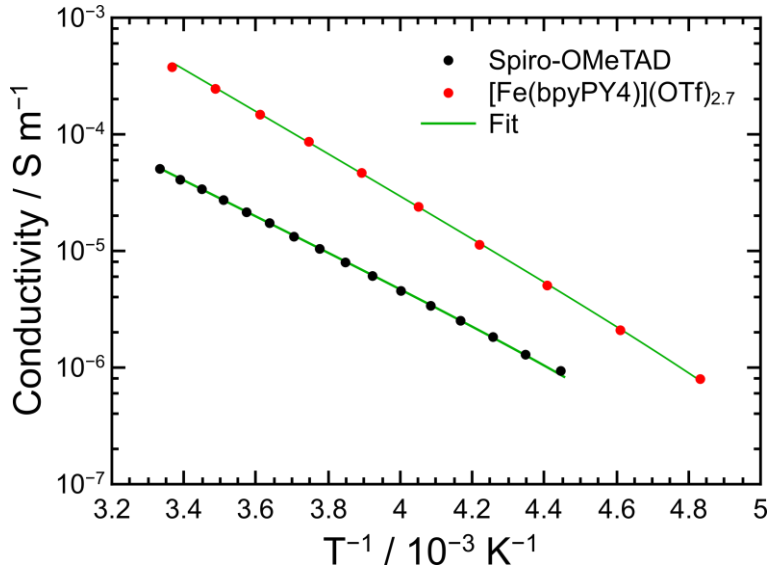

Figure S6. Arrhenius plot of the conductivity of the [Fe(bpyPY4)](OTf)$_{2.7}$ (*red*) and 10% oxidized spiro-OMeTAD (*black*) thin films drop-cast onto IDA electrodes.

Cyclic voltammetry

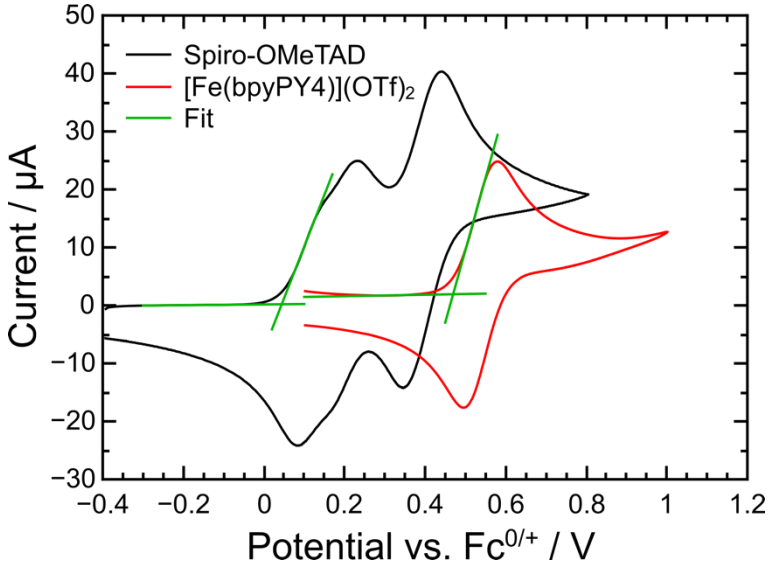

Figure S7. Cyclic voltammograms (scan rate 0.1 V s^{-1}) obtained with a gold electrode (3 mm diameter) for oxidation of 2.3 mM spiro-OMeTAD in acetonitrile:chlorobenzene 3.38:1 vol. (0.077 M *n*-Bu_4NPF_6) (*black*) and 3 mM $[Fe(bpyPY4)](OTf)_2$ in acetonitrile (0.1 M *n*-Bu_4NPF_6) (*red*). Measurements were undertaken inside a nitrogen-filled glove-box. *Green* lines show the estimated oxidation onsets.

Photoelectron spectroscopy in air

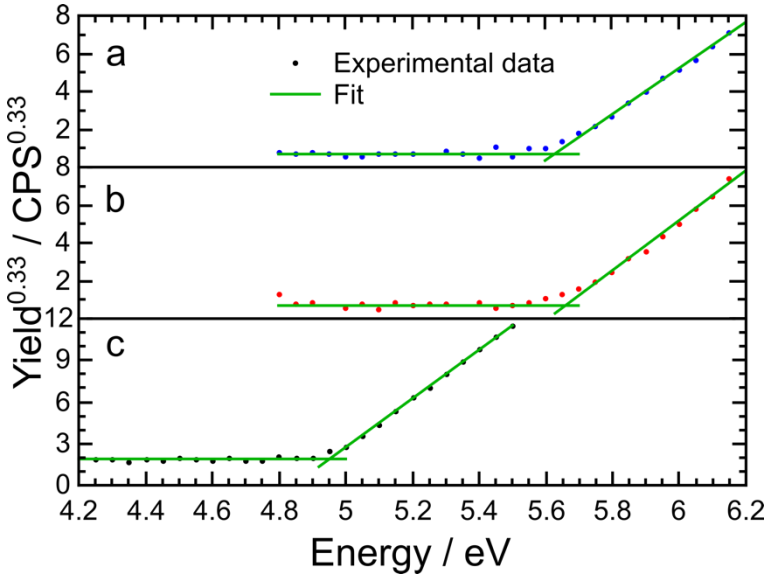

Figure S8. PESA measurements for the (a) $FAPbBr_3$, (b) $[Fe(bpyPY4)](OTf)_{2.5}$ and (c) spiro-OMeTAD spin-coated films. $FAPbBr_3$ was deposited on FTO|c-TiO_2, while $[Fe(bpyPY4)](OTf)_{2.5}$ and spiro-OMeTAD were deposited on FTO|c-TiO_2|$FAPbBr_3$. *Green* lines show linear fits used to derive E_{VB}/HOMO.

Ultraviolet photoelectron spectroscopy

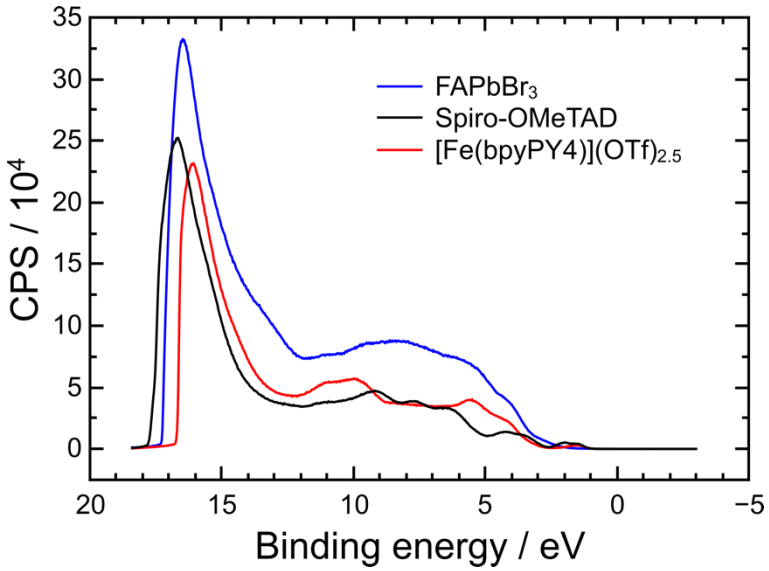

Figure S9. UPS data for the spin-coated $FAPbBr_3$ (*blue*), spiro-OMeTAD (*black*) and $[Fe(bpyPY4)](OTf)_{2.5}$ (*red*) films. As a support, a compact TiO_2 layer on FTO was used for $FAPbBr_3$, while HTMs were deposited on FTO|c-TiO_2|$FAPbBr_3$.

Energy levels

Table S1. Highest occupied molecular orbital (HOMO) positions for $[Fe(bpyPY4)](OTf)_{2.5}$ and spiro-OMeTAD and valence band edge (E_{VB}) energy level and band gap for $FAPbBr_3$. All values are referred to vacuum.

Material	HOMO (eV)	HOMO / E_{VB} (eV)		E_g (eV)
	(Voltammetry)[a]	(UPS)[b]	(PESA)[b]	(Tauc)[c]
$FAPbBr_3$		−5.83	−5.62	2.28
$[Fe(bpyPY4)](OTf)_{2.5}$	−5.57	−5.46	−5.67	
Spiro-OMeTAD	−5.14	−4.69	−4.95	

(a) Calculated using the onset of the first oxidation peak (shown in Figure S7) assuming that the formal potential of the $Fc^{0/+}$ redox couple is 5.1 eV.[S4] (b) Derived from the data shown in Figures S8 and S9. (c) Derived from the Tauc plot exemplified in Figure S10.

UV-Vis spectrum and Tauc plot for $FAPbBr_3$

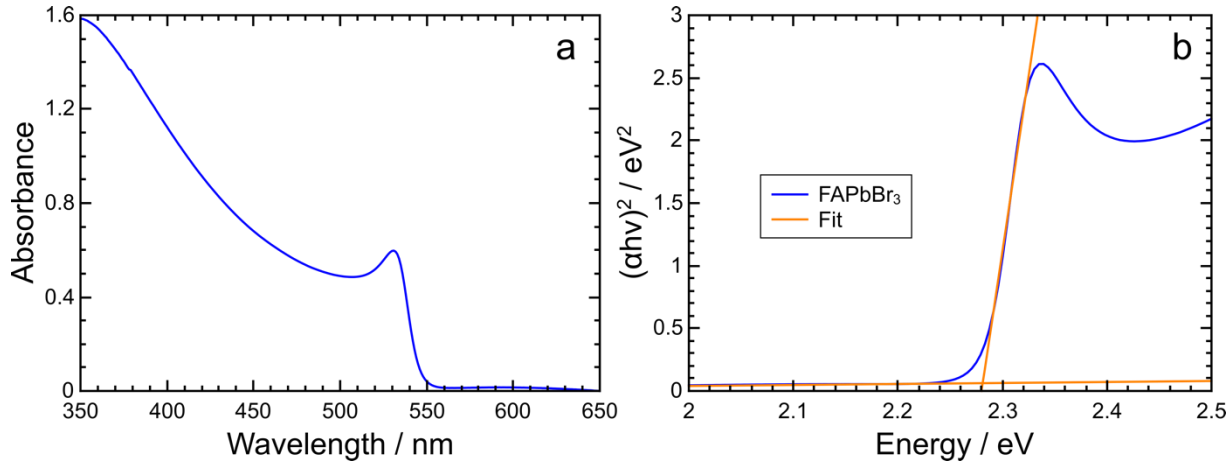

Figure S10. (a) UV-Vis absorption spectrum of the $FAPbBr_3$ perovskite film spin-coated on glass. (b) Tauc plot constructed using the data in panel **a** (*blue*) and linear fit used to derive E_g (*orange*).

Photoluminescence quenching

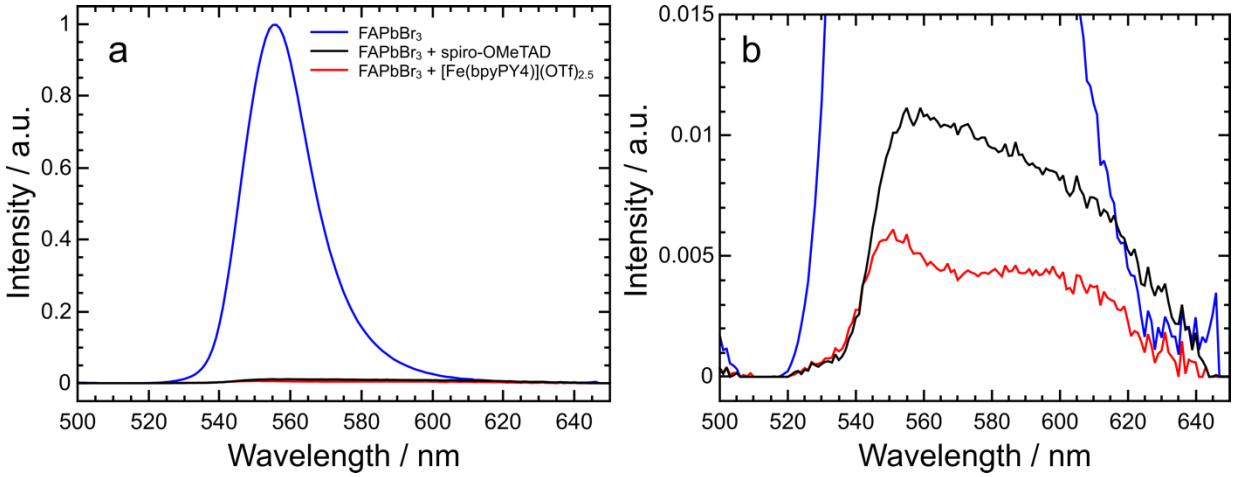

Figure S11. Photoluminescence spectra of the $FAPbBr_3$ film spin-coated on a glass substrate without (*blue*) and with the spiro-OMeTAD (*black*) or $[Fe(bpyPY4)](OTf)_{2.5}$ (*red*) films deposited on top. Illumination was from the glass side. Data are normalized to the peak value for the unmodified $FAPbBr_3$ film. Panels **a** and **b** show full and low intensity ranges of the ordinate axis, respectively.

Cross-sectional SEM images

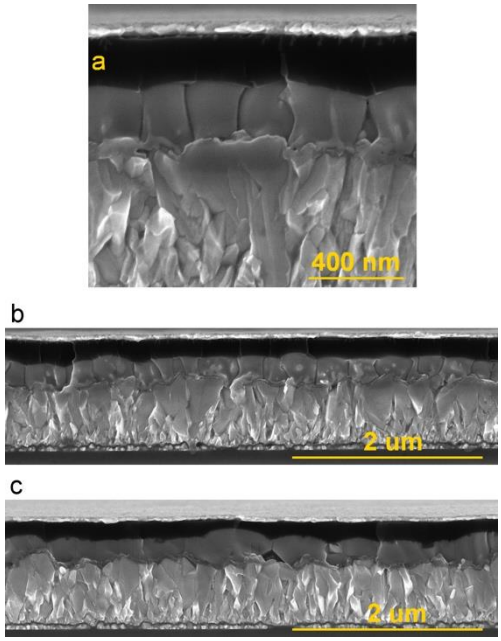

Figure S12. Cross-sectional SEM images of the FTO|c-TiO_2|$FAPbBr_3$|HTM|Au devices based on the (a, b) spiro-OMeTAD and (c) $[Fe(bpyPY4)](OTf)_{2.5}$ HTM.

Surface SEM images and composition of $FAPbBr_3$

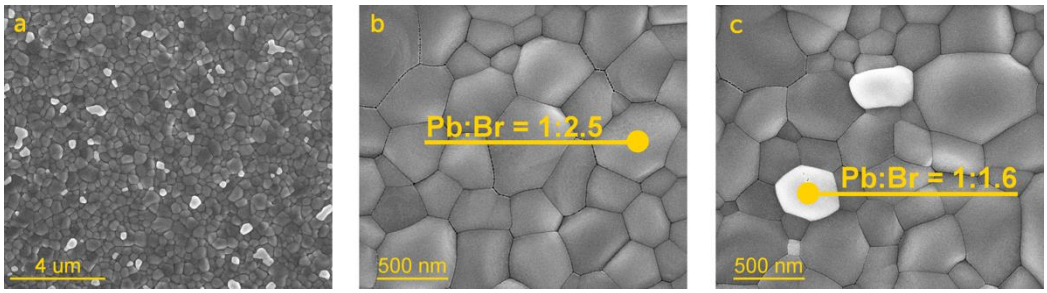

Figure S13. (a) Lower (20k ×) and (b, c) higher (120k ×) magnification SEM images of the $FAPbBr_3$ perovskite surface. The lighter-colored grains are comprised of $PbBr_2$. In panels **b** and **c**, the atomic Pb:Br ratios were derived from the energy dispersive X-ray analysis (EDX) centered on the areas marked with circles. Note that EDX is not a fully quantitative analytic method. Furthermore, the size of the $PbBr_2$ grains is notably smaller than the depth and breadth of the point EDX analysis under employed conditions, which results in a lower than expected Pb:Br ratio. The slight inconsistency of the EDX results obtained for the $FAPbBr_3$ grains with the expected stoichiometry is due to damage of the perovskite by the electron beam.

XRD patterns for $FAPbBr_3$ and $PbBr_2$ films

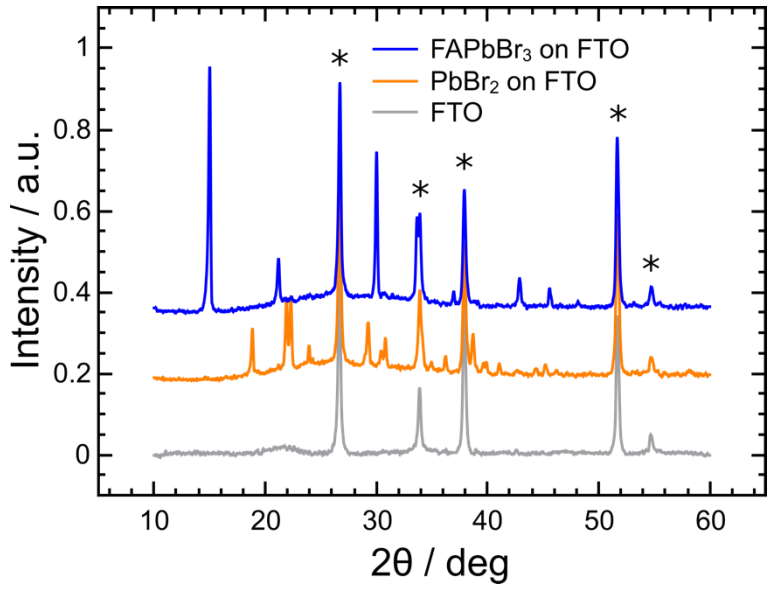

Figure S14. XRD patterns of bare FTO (*gray*), and FTO modified with $FAPbBr_3$ (*blue*) or $PbBr_2$ (*orange*) films. No $PbBr_2$ peaks are detected for the perovskite film. The * symbols show peaks corresponding to the FTO substrate.

Quasi-steady-state power measurements

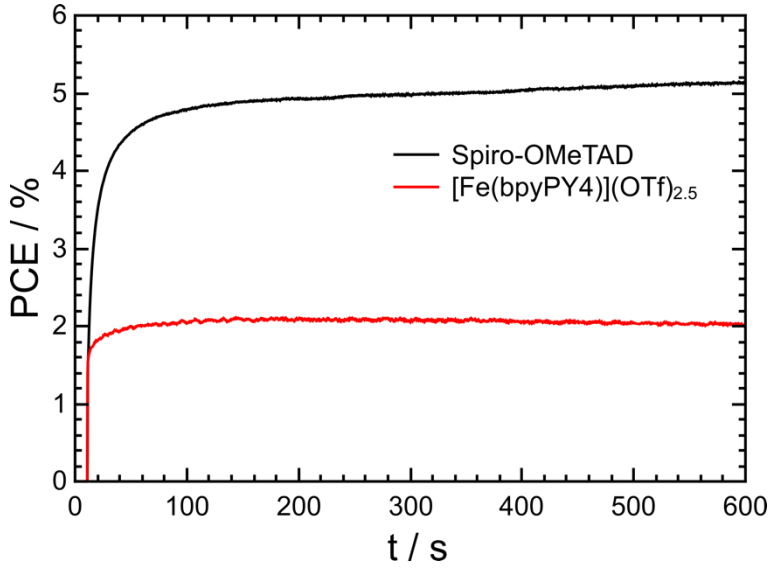

Figure S15. Maximum-power-point PCE transients measured under 1 sun AM1.5G irradiation for the best-performing spiro-OMeTAD-based (applied voltage 926 mV) and $[Fe(bpyPY4)](OTf)_{2.5}$-based (applied voltage 529 mV) solar cells.

Complete *J-V* scan data

Table S2. Complete list of photovoltaic parameters[a] for $FAPbBr_3$ perovskite solar cells with different HTMs under 1 sun AM1.5G irradiation.

Hole transporting material	V_{OC} (mV)	J_{SC} (mA cm^{-2})	FF (%)	PCE (%)
Spiro-OMeTAD (best, SC → FB)	1368	6.6	48	4.3
Spiro-OMeTAD (best, FB → SC)	1308	6.6	60	5.2
Spiro-OMeTAD (average, SC → FB)	1310 ± 50	6.4 ± 0.3	50 ± 4	4.2 ± 0.3
Spiro-OMeTAD (average, FB → SC)	1290 ± 40	6.3 ± 0.4	61 ± 6	4.9 ± 0.4
[Fe(bpyPY4)](OTf)$_{2.5}$ (best, SC → FB)	855	6.0	42	2.2
[Fe(bpyPY4)](OTf)$_{2.5}$ (best, FB → SC)	889	6.0	50	2.7
[Fe(bpyPY4)](OTf)$_{2.5}$ (average, SC → FB)	760 ± 60	6.1 ± 0.3	42 ± 2	2.0 ± 0.3
[Fe(bpyPY4)](OTf)$_{2.5}$ (average, FB → SC)	820 ± 60	6.1 ± 0.2	47 ± 2	2.4 ± 0.3

[a] Derived from the *J-V* curves (scan rate = 10 mV s^{-1}) for seven spiro-OMeTAD-based and 15 [Fe(bpyPY4)](OTf)$_{2.5}$-based devices. V_{OC}, open-circuit voltage; J_{SC}, short-circuit current density; FF, fill factor; SC, short-circuit; FB, forward bias.

FTO|c-TiO_2|[Fe(bpyPY4)](OTf)$_{2.5}$|Au diode

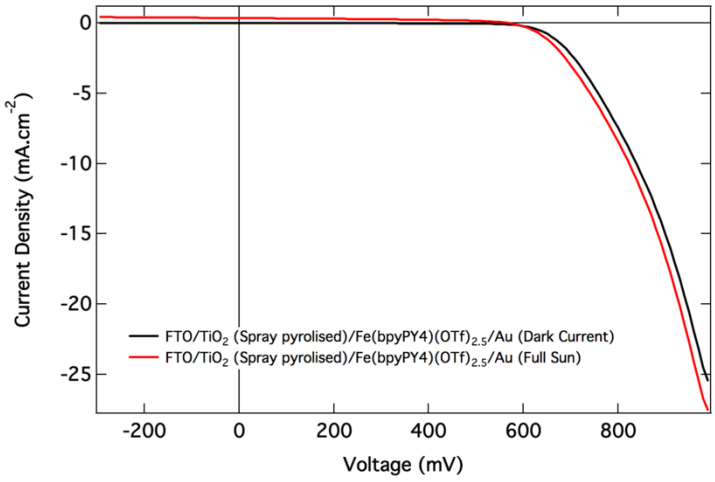

Figure S16. *J-V* characterization of the FTO|c-TiO_2|[Fe(bpyPY4)](OTf)$_{2.5}$|Au diode, showing good rectifying properties of Fe(bpyPY4)](OTf)$_{2.5}$ and no electron injection under 1 sun irradiation. The small photocurrent (*ca* 300 μA cm^{-2} at −0.3 V) is generated by titania as confirmed in control experiments undertaken with no Fe(bpyPY4)](OTf)$_{2.5}$ present.

Long-term stability

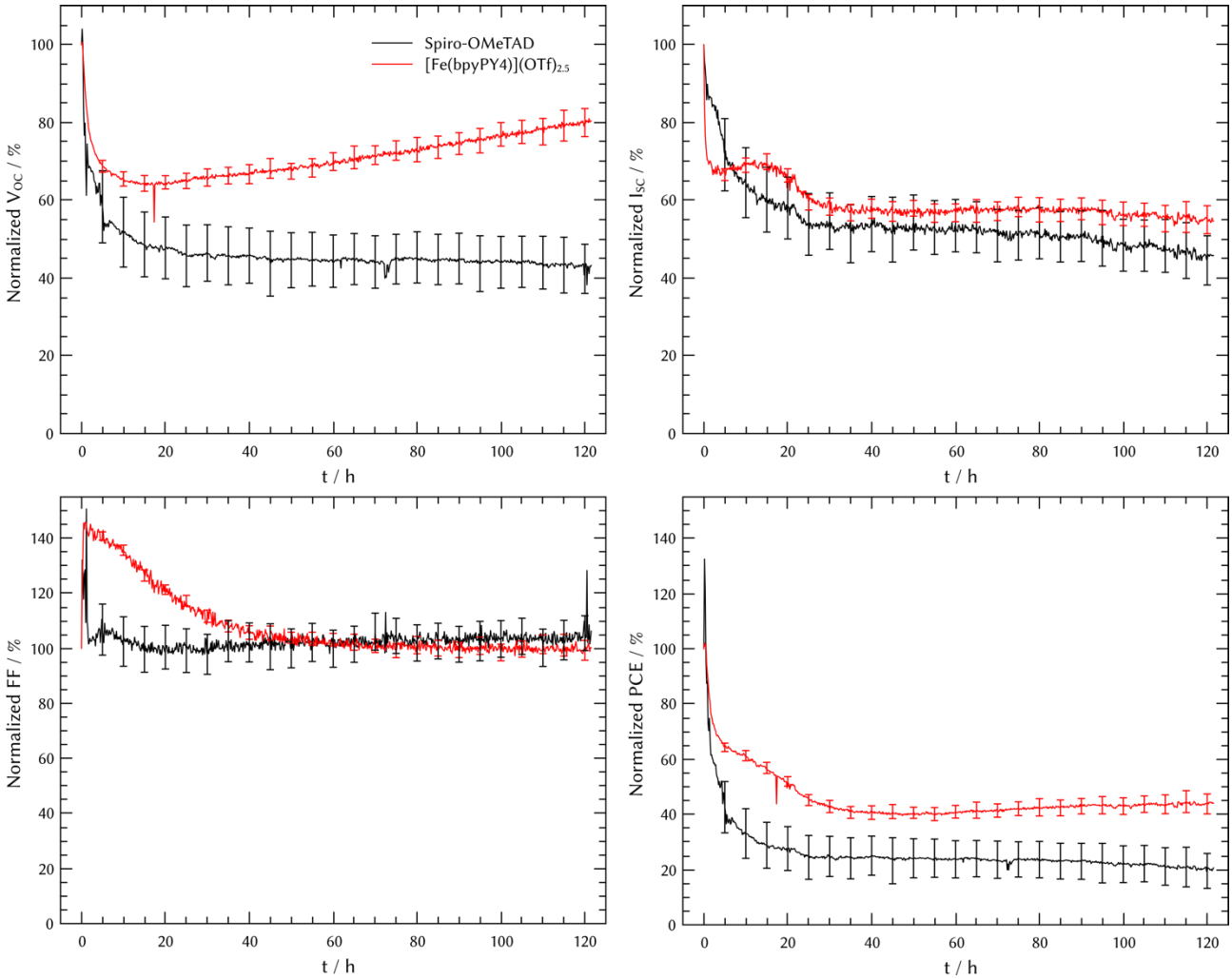

Figure S17. Evolution of the photovoltaic parameters of encapsulated $FAPbBr_3$-based planar solar cells fabricated with spiro-OMeTAD (*black*) or $[Fe(bpyPY4)](OTf)_{2.5}$ (*red*) as a HTM under continuous 1 sun irradiation at 25 °C (actual cell temperature was higher due to continuous irradiation) and 20% relative humidity. Curves represent average values for five devices; standard deviation error bars are shown every 30 experimental points for clarity. All parameters are normalized to the corresponding initial values at $t = 0$.

Electrochemical impedance spectroscopy

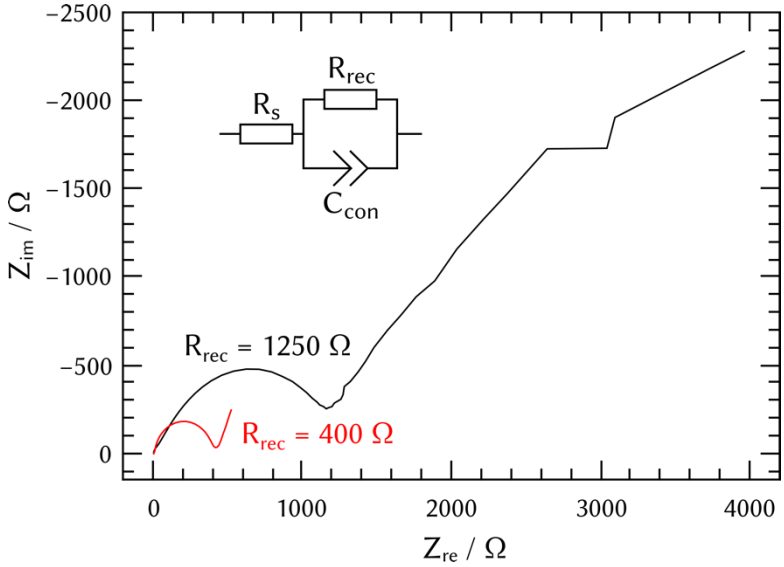

Figure S18. Nyquist impedance spectra for FTO|c-TiO_2|$FAPbBr_3$|HTM|Au devices with spiro-OMeTAD (*black*) or [Fe(bpyPY4)](OTf)$_{2.5}$ (*red*) as a HTM. Measurements were performed under illumination (27 mW cm^{-2}) with an applied potential of 700 mV for the device with spiro-OMeTAD and of 400 mV for the device with [Fe(bpyPY4)](OTf)$_{2.5}$, in the frequency range 1 Hz – 4 MHz. The recombination resistance (R_{rec}) was calculated by fitting the semicircle in the middle frequency range ($50 < Z_{Re} < 1200$ Ω for spiro-OMeTAD and $15 < Z_{Re} < 400$ Ω for [Fe(bpyPY4)](OTf)$_{2.5}$) to the simplified version of the equivalent circuit introduced by Pascoe *et al.*[S5] (R_s - series resistance; C_{con} - constant phase shift element used to simulate capacitive behavior at the interface). R_{rec} does not contribute to the low frequency range, which facilitates analysis of the data based on the equivalent circuit shown in the figure.

References

(S1) Kashif, M. K.; Nippe, M.; Duffy, N. W.; Forsyth, C. M.; Chang, C. J.; Long, J. R.; Spiccia, L.; Bach, U. Stable Dye-Sensitized Solar Cell Electrolytes Based on Cobalt(II)/(III) Complexes of a Hexadentate Pyridyl Ligand. *Angew. Chem. Int. Ed.* **2013**, *52* (21), 5527–5531.

(S2) Cappel, U. B.; Daeneke, T.; Bach, U. Oxygen-Induced Doping of Spiro-MeOTAD in Solid-State Dye-Sensitized Solar Cells and Its Impact on Device Performance. *Nano Lett.* **2012**, *12* (9), 4925–4931.

(S3) Huang, F.; Dkhissi, Y.; Huang, W.; Xiao, M.; Benesperi, I.; Rubanov, S.; Zhu, Y.; Lin, X.; Jiang, L.; Zhou, Y.; et al. Gas-assisted preparation of lead iodide perovskite films consisting of a monolayer of single crystalline grains for high efficiency planar solar cells. *Nano Energy* **2014**, *10*, 10–18.

(S4) Cardona, C. M.; Li, W.; Kaifer, A. E.; Stockdale, D.; Bazan, G. C. Electrochemical Considerations for Determining Absolute Frontier Orbital Energy Levels of Conjugated Polymers for Solar Cell Applications. *Adv. Mater.* **2011**, *23* (20), 2367–2371.

(S5) Pascoe, A. R.; Duffy, N. W.; Scully, A. D.; Huang, F.; Cheng, Y.-B. Insights into Planar $CH_3NH_3PbI_3$ Perovskite Solar Cells Using Impedance Spectroscopy. *J. Phys. Chem. C* **2015**, *119* (9), 4444–4453.

Complete single crystal XRD data refinement for $[Fe(bpyPY4)](OTf)_2$

Table 1. Crystal data and structure refinement for $[Fe(bpyPY4)](OTf)_2$.

Identification code	mx05_15
Empirical formula	C36 H28 F6 Fe N6 O6 S2
Formula weight	874.61
Temperature	123.01(10) K
Wavelength	0.71073 A
Crystal system, space group	Triclinic, P-1
Unit cell dimensions	a = 8.3101(3) A alpha = 114.636(4) deg. b = 10.4017(3) A beta = 95.979(3) deg. c = 11.6371(5) A gamma = 98.975(3) deg.
Volume	886.96(6) A^3
Z, Calculated density	1, 1.637 Mg/m^3
Absorption coefficient	0.632 mm^-1
F(000)	446
Crystal size	0.20 x 0.17 x 0.09 mm
Theta range for data collection	1.960 to 30.467 deg.
Limiting indices	-11<=h<=11, -14<=k<=14, -15<=l<=16
Reflections collected / unique	13623 / 4881 [R(int) = 0.0292]
Completeness to theta = 25.242	100.0 %
Absorption correction	Semi-empirical from equivalents
Max. and min. transmission	1.00000 and 0.86358
Refinement method	Full-matrix least-squares on F^2
Data / restraints / parameters	4881 / 30 / 413
Goodness-of-fit on F^2	1.059
Final R indices [I>2sigma(I)]	R1 = 0.0421, wR2 = 0.0960
R indices (all data)	R1 = 0.0597, wR2 = 0.1069
Extinction coefficient	n/a
Largest diff. peak and hole	0.380 and -0.456 e.A^-3

Table 2. Atomic coordinates (x 10^4) and equivalent isotropic displacement parameters (A^2 x 10^3) for $[Fe(bpyPY4)](OTf)_2$. U(eq) is defined as one third of the trace of the orthogonalized Uij tensor.

	x	y	z	U(eq)
Fe(1)	0	10000	5000	21(1)
S(1)	3430(1)	5842(1)	8173(1)	34(1)
F(1)	3629(9)	8705(7)	9459(4)	59(1)
F(1')	3318(9)	8451(7)	8834(6)	73(2)
F(2)	1407(10)	7613(7)	8046(9)	62(2)

F(2')	1095(12)	6948(7)	7696(11)	89(3)
F(3)	3721(4)	8107(4)	7479(3)	47(1)
F(3')	3179(6)	7145(5)	6826(4)	69(1)
O(1)	2674(2)	5801(2)	9213(2)	48(1)
O(2)	5213(2)	6244(2)	8450(2)	35(1)
O(3)	2725(6)	4979(5)	6797(4)	53(1)
O(3')	2757(6)	4436(4)	7091(4)	44(1)
N(1)	941(2)	10633(2)	3781(2)	24(1)
N(2)	-2022(19)	9055(9)	3657(14)	22(2)
N(3)	2010(20)	10568(9)	6231(13)	16(2)
N(4)	1146(6)	8450(6)	4079(5)	21(1)
N(5)	-636(6)	11847(6)	5789(5)	22(1)
C(1)	3007(12)	7651(10)	8254(10)	34(2)
C(1')	2718(17)	7117(10)	7886(12)	49(2)
C(2)	1859(3)	11987(2)	4173(2)	31(1)
C(3)	2573(3)	12433(2)	3351(2)	35(1)
C(4)	2337(3)	11468(3)	2067(2)	35(1)
C(5)	1364(3)	10096(2)	1649(2)	30(1)
C(6)	682(2)	9689(2)	2516(2)	23(1)
C(7)	-380(2)	8155(2)	2108(2)	23(1)
C(8)	-593(3)	7218(2)	657(2)	29(1)
C(9)	-2020(20)	8270(20)	2381(17)	29(4)
C(10)	-3506(14)	7558(8)	1525(10)	31(2)
C(11)	-4966(6)	7634(7)	1899(5)	52(2)
C(12)	-4996(6)	8451(7)	3183(5)	57(2)
C(13)	-3498(6)	9167(6)	4024(4)	42(1)
C(14)	2098(14)	11567(17)	7453(16)	14(2)
C(15)	3554(15)	11970(7)	8363(10)	22(1)
C(16)	4876(4)	11320(4)	8027(4)	20(1)
C(17)	4631(5)	10130(5)	6848(4)	27(1)
C(18)	3164(5)	9762(4)	5980(4)	22(1)
C(19)	2619(5)	8470(4)	4738(4)	25(1)
C(20)	3483(6)	7386(5)	4214(4)	34(1)
C(21)	2856(7)	6323(5)	2969(4)	38(1)
C(22)	1524(8)	6460(7)	2245(7)	27(1)
C(23)	747(10)	7607(10)	2785(8)	20(1)
C(24)	-1406(5)	12416(5)	5103(4)	28(1)
C(25)	-1957(6)	13684(5)	5650(4)	35(1)
C(26)	-1753(6)	14381(5)	6967(4)	34(1)
C(27)	-939(7)	13823(8)	7687(8)	29(1)
C(28)	-401(9)	12567(9)	7071(8)	16(1)

Table 3. Bond lengths [A] and angles [deg] for $[Fe(bpyPY4)](OTf)_2$.

Fe(1)-N(1)#1	1.9764(17)
Fe(1)-N(1)	1.9764(17)
Fe(1)-N(2)	1.972(15)
Fe(1)-N(3)	1.920(16)
Fe(1)-N(4)	1.977(6)
Fe(1)-N(5)	1.939(6)
S(1)-O(1)	1.4338(18)
S(1)-O(2)	1.4382(16)
S(1)-O(3)	1.468(4)
S(1)-O(3')	1.449(4)
S(1)-C(1)	1.933(10)
S(1)-C(1')	1.670(13)
F(1)-C(1)	1.352(9)
F(1')-C(1')	1.336(9)
F(2)-C(1)	1.317(13)
F(2')-C(1')	1.316(17)
F(3)-C(1)	1.331(12)
F(3')-C(1')	1.340(14)
N(1)-C(2)	1.353(3)
N(1)-C(6)	1.357(2)
N(2)-C(9)	1.36(2)
N(2)-C(13)	1.347(16)
N(3)-C(14)	1.35(2)
N(3)-C(18)	1.344(13)
N(4)-C(19)	1.368(6)
N(4)-C(23)	1.360(10)
N(5)-C(24)	1.342(7)

N(5)-C(28)	1.337(10)
C(2)-C(3)	1.373(3)
C(3)-C(4)	1.381(3)
C(4)-C(5)	1.381(3)
C(5)-C(6)	1.385(3)
C(6)-C(7)	1.547(3)
C(7)-C(8)	1.531(3)
C(7)-C(9)	1.446(18)
C(7)-C(14)#1	1.593(15)
C(7)-C(23)	1.486(10)
C(7)-C(28)#1	1.587(9)
C(9)-C(10)	1.38(2)
C(10)-C(11)	1.334(13)
C(11)-C(12)	1.382(7)
C(12)-C(13)	1.383(7)
C(14)-C(15)	1.402(18)
C(15)-C(16)	1.385(11)
C(16)-C(17)	1.380(5)
C(17)-C(18)	1.389(5)
C(18)-C(19)	1.468(5)
C(19)-C(20)	1.388(5)
C(20)-C(21)	1.386(6)
C(21)-C(22)	1.383(9)
C(22)-C(23)	1.391(13)
C(24)-C(25)	1.380(6)
C(25)-C(26)	1.372(6)
C(26)-C(27)	1.381(9)
C(27)-C(28)	1.374(12)

N(1)-Fe(1)-N(1)#1	180.00(8)
N(1)-Fe(1)-N(4)	77.13(14)
N(1)#1-Fe(1)-N(4)	102.87(14)
N(2)-Fe(1)-N(1)#1	94.1(5)
N(2)-Fe(1)-N(1)	85.9(5)
N(2)-Fe(1)-N(4)	92.0(4)
N(3)-Fe(1)-N(1)#1	82.6(4)
N(3)-Fe(1)-N(1)	97.5(4)
N(3)-Fe(1)-N(2)	169.6(5)
N(3)-Fe(1)-N(4)	79.2(4)
N(3)-Fe(1)-N(5)	95.3(3)
N(5)-Fe(1)-N(1)	88.48(14)
N(5)-Fe(1)-N(1)#1	91.52(14)
N(5)-Fe(1)-N(2)	94.7(3)
N(5)-Fe(1)-N(4)	163.67(13)
O(1)-S(1)-O(2)	115.18(11)
O(1)-S(1)-O(3)	125.8(2)
O(1)-S(1)-O(3')	105.44(19)
O(1)-S(1)-C(1)	99.6(3)
O(1)-S(1)-C(1')	104.1(5)
O(2)-S(1)-O(3)	113.7(2)
O(2)-S(1)-O(3')	113.8(2)
O(2)-S(1)-C(1)	98.1(3)
O(2)-S(1)-C(1')	108.1(5)
O(3)-S(1)-C(1)	95.6(4)
O(3')-S(1)-C(1')	109.6(4)
C(2)-N(1)-Fe(1)	121.82(14)
C(2)-N(1)-C(6)	118.49(18)
C(6)-N(1)-Fe(1)	119.68(13)
C(9)-N(2)-Fe(1)	124.2(12)
C(13)-N(2)-Fe(1)	118.0(9)
C(13)-N(2)-C(9)	117.8(13)
C(14)-N(3)-Fe(1)	119.1(11)
C(18)-N(3)-Fe(1)	120.2(7)
C(18)-N(3)-C(14)	118.9(13)
C(19)-N(4)-Fe(1)	116.4(4)
C(23)-N(4)-Fe(1)	123.1(6)
C(23)-N(4)-C(19)	118.9(6)
C(24)-N(5)-Fe(1)	122.9(4)
C(28)-N(5)-Fe(1)	119.9(5)
C(28)-N(5)-C(24)	117.1(6)
F(1)-C(1)-S(1)	108.5(7)
F(2)-C(1)-S(1)	112.0(7)
F(2)-C(1)-F(1)	106.3(8)
F(2)-C(1)-F(3)	108.8(8)
F(3)-C(1)-S(1)	115.3(6)

F(3)-C(1)-F(1)	105.5(7)
F(1')-C(1')-S(1)	113.0(10)
F(1')-C(1')-F(3')	106.0(10)
F(2')-C(1')-S(1)	115.3(9)
F(2')-C(1')-F(1')	105.9(10)
F(2')-C(1')-F(3')	106.0(11)
F(3')-C(1')-S(1)	110.1(8)
N(1)-C(2)-C(3)	122.75(19)
C(2)-C(3)-C(4)	118.9(2)
C(3)-C(4)-C(5)	118.8(2)
C(4)-C(5)-C(6)	120.2(2)
N(1)-C(6)-C(5)	120.75(18)
N(1)-C(6)-C(7)	116.79(17)
C(5)-C(6)-C(7)	122.45(17)
C(6)-C(7)-C(14)#1	104.4(6)
C(6)-C(7)-C(28)#1	109.9(3)
C(8)-C(7)-C(6)	111.13(17)
C(8)-C(7)-C(14)#1	112.4(5)
C(8)-C(7)-C(28)#1	112.4(3)
C(9)-C(7)-C(6)	109.2(7)
C(9)-C(7)-C(8)	106.7(7)
C(9)-C(7)-C(14)#1	6.1(11)
C(9)-C(7)-C(23)	121.4(9)
C(9)-C(7)-C(28)#1	107.2(9)
C(23)-C(7)-C(6)	99.9(3)
C(23)-C(7)-C(8)	108.3(4)
C(23)-C(7)-C(14)#1	119.8(7)
C(23)-C(7)-C(28)#1	14.6(4)
C(28)#1-C(7)-C(14)#1	106.1(7)
N(2)-C(9)-C(7)	113.0(13)
N(2)-C(9)-C(10)	120.0(15)
C(10)-C(9)-C(7)	126.6(14)
C(11)-C(10)-C(9)	122.0(11)
C(10)-C(11)-C(12)	119.0(6)
C(11)-C(12)-C(13)	118.1(4)
N(2)-C(13)-C(12)	122.9(7)
N(3)-C(14)-C(7)#1	116.7(10)
N(3)-C(14)-C(15)	119.4(14)
C(9)#1-C(14)-N(3)	159(8)
C(9)#1-C(14)-C(7)#1	45(7)
C(9)#1-C(14)-C(15)	81(8)
C(15)-C(14)-C(7)#1	121.0(12)
C(16)-C(15)-C(14)	120.4(10)
C(17)-C(16)-C(15)	118.1(5)
C(16)-C(17)-C(18)	118.8(3)
N(3)-C(18)-C(17)	122.0(7)
N(3)-C(18)-C(19)	111.4(6)
C(17)-C(18)-C(19)	126.6(3)
N(4)-C(19)-C(18)	112.5(4)
N(4)-C(19)-C(20)	121.3(4)
C(20)-C(19)-C(18)	126.1(4)
C(21)-C(20)-C(19)	118.0(4)
C(22)-C(21)-C(20)	119.6(5)
C(21)-C(22)-C(23)	120.4(7)
N(4)-C(23)-C(7)	113.1(7)
N(4)-C(23)-C(22)	118.6(8)
C(22)-C(23)-C(7)	128.0(7)
N(5)-C(24)-C(25)	123.6(4)
C(26)-C(25)-C(24)	118.3(4)
C(25)-C(26)-C(27)	118.8(5)
C(28)-C(27)-C(26)	119.4(7)
N(5)-C(28)-C(7)#1	117.7(7)
N(5)-C(28)-C(27)	122.7(8)
C(23)#1-C(28)-N(5)	112(3)
C(23)#1-C(28)-C(7)#1	68(2)
C(23)#1-C(28)-C(27)	85(3)
C(27)-C(28)-C(7)#1	119.4(6)

Symmetry transformations used to generate equivalent atoms:
#1 -x,-y+2,-z+1

Table 4. Anisotropic displacement parameters (A^2 x 10^3) for [Fe(bpyPY4)](OTf)$_2$.

The anisotropic displacement factor exponent takes the form:
-2 pi^2 [h^2 a*^2 U11 + ... + 2 h k a* b* U12]

	U11	U22	U33	U23	U13	U12
Fe(1)	22(1)	19(1)	17(1)	3(1)	-1(1)	7(1)
S(1)	31(1)	30(1)	27(1)	0(1)	2(1)	5(1)
F(1)	76(3)	35(2)	47(3)	0(2)	11(3)	18(2)
F(1')	113(5)	32(3)	84(5)	26(4)	29(5)	34(4)
F(2)	45(3)	84(4)	81(4)	49(4)	20(3)	37(3)
F(2')	56(4)	112(6)	141(8)	89(6)	19(4)	44(5)
F(3)	49(2)	53(2)	55(2)	38(2)	11(2)	16(2)
F(3')	97(3)	76(3)	63(2)	55(2)	20(2)	23(2)
O(1)	43(1)	50(1)	61(1)	34(1)	20(1)	10(1)
O(2)	32(1)	34(1)	38(1)	15(1)	8(1)	8(1)
O(3)	63(3)	34(2)	34(2)	-6(2)	-7(2)	5(2)
O(3')	63(3)	24(2)	28(2)	1(2)	4(2)	-1(2)
N(1)	22(1)	20(1)	22(1)	3(1)	2(1)	5(1)
N(2)	15(2)	21(5)	17(3)	-1(4)	4(2)	2(4)
N(3)	23(2)	12(4)	13(3)	4(3)	3(2)	5(3)
N(4)	26(3)	20(2)	14(2)	4(2)	4(2)	10(2)
N(5)	25(3)	26(3)	18(2)	10(2)	8(2)	10(2)
C(1)	35(4)	34(5)	39(6)	18(4)	10(4)	18(4)
C(1')	60(6)	45(6)	57(7)	31(5)	21(5)	19(5)
C(2)	31(1)	23(1)	29(1)	4(1)	-1(1)	4(1)
C(3)	34(1)	25(1)	42(1)	13(1)	2(1)	1(1)
C(4)	31(1)	37(1)	37(1)	15(1)	9(1)	5(1)
C(5)	26(1)	32(1)	27(1)	7(1)	7(1)	7(1)
C(6)	19(1)	22(1)	24(1)	4(1)	4(1)	7(1)
C(7)	24(1)	19(1)	20(1)	3(1)	1(1)	6(1)
C(8)	32(1)	26(1)	20(1)	2(1)	1(1)	6(1)
C(9)	38(5)	29(5)	16(4)	7(4)	6(3)	7(3)
C(10)	24(2)	37(5)	18(3)	3(4)	0(2)	-2(4)
C(11)	25(2)	74(4)	32(3)	1(3)	-2(2)	8(2)
C(12)	25(2)	92(5)	34(3)	8(3)	9(2)	10(3)
C(13)	28(2)	66(4)	23(2)	9(2)	5(2)	12(2)
C(14)	9(2)	15(3)	12(4)	1(3)	2(2)	-1(2)
C(15)	28(3)	16(3)	16(3)	4(3)	1(2)	-1(3)
C(16)	17(2)	22(2)	20(2)	8(2)	0(1)	4(1)
C(17)	22(2)	39(2)	20(2)	9(2)	4(2)	15(2)
C(18)	22(2)	26(2)	19(2)	8(2)	5(1)	12(2)
C(19)	29(2)	24(2)	23(2)	9(2)	4(2)	11(2)
C(20)	38(2)	33(2)	27(2)	8(2)	4(2)	19(2)
C(21)	54(3)	29(2)	29(2)	4(2)	7(2)	25(2)
C(22)	36(4)	20(3)	19(2)	0(2)	7(3)	12(3)
C(23)	24(3)	19(3)	13(2)	6(2)	7(2)	-1(2)
C(24)	36(2)	36(2)	18(2)	12(2)	10(2)	22(2)
C(25)	44(2)	38(2)	33(2)	18(2)	10(2)	26(2)
C(26)	43(3)	21(2)	35(2)	7(2)	5(2)	19(2)
C(27)	28(3)	26(3)	24(2)	3(2)	3(3)	6(3)
C(28)	19(3)	16(2)	16(2)	8(2)	9(2)	6(2)

Table 5. Hydrogen coordinates (x 10^4) and isotropic displacement parameters (A^2 x 10^3) for [Fe(bpyPY4)](OTf)$_2$.

	x	y	z	U(eq)
H(2)	2017	12658	5055	37
H(3)	3219	13390	3660	42
H(4)	2835	11743	1481	43
H(5)	1162	9428	764	36
H(8A)	-1256	6250	427	44
H(8B)	499	7137	424	44
H(8C)	-1159	7668	192	44
H(10)	-3486	6997	643	37
H(11)	-5971	7133	1291	63

H(12)	-6017	8520	3478	68
H(13)	-3511	9764	4901	51
H(15)	3634	12693	9215	27
H(16)	5922	11683	8593	24
H(17)	5452	9572	6633	33
H(20)	4473	7374	4694	40
H(21)	3340	5506	2616	46
H(22)	1136	5766	1373	33
H(24)	-1581	11918	4191	34
H(25)	-2465	14064	5128	42
H(26)	-2163	15232	7375	40
H(27)	-753	14303	8601	35

Complete single crystal XRD data refinement for $[Fe(bpyPY4)](OTf)_3$

Table 1. Crystal data and structure refinement for $[Fe(bpyPY4)](OTf)_3 \cdot MeCN$.

Identification code	shelx
Empirical formula	C39 H31 F9 Fe N7 O9 S3
Formula weight	1064.74
Temperature	123(2) K
Wavelength	0.71073 A
Crystal system, space group	Monoclinic, P2(1)/n
Unit cell dimensions	a = 18.2511(10) A alpha = 90 deg. b = 13.9494(5) A beta = 117.614(7) deg. c = 19.6316(10) A gamma = 90 deg.
Volume	4428.7(4) A^3
Z, Calculated density	4, 1.597 Mg/m^3
Absorption coefficient	0.582 mm^-1
F(000)	2164
Crystal size	0.25 x 0.08 x 0.05 mm
Theta range for data collection	3.399 to 25.999 deg.
Limiting indices	-22<=h<=22, -17<=k<=13, -23<=l<=24
Reflections collected / unique	36252 / 8695 [R(int) = 0.0345]
Completeness to theta = 25.242	99.8 %
Absorption correction	Semi-empirical from equivalents
Max. and min. transmission	1.00000 and 0.98482
Refinement method	Full-matrix least-squares on F^2
Data / restraints / parameters	8695 / 0 / 678
Goodness-of-fit on F^2	1.023
Final R indices [I>2sigma(I)]	R1 = 0.0596, wR2 = 0.1586
R indices (all data)	R1 = 0.0782, wR2 = 0.1739
Extinction coefficient	n/a
Largest diff. peak and hole	2.795 and -0.739 e.A^-3

Table 2. Atomic coordinates (x 10^4) and equivalent isotropic displacement parameters (A^2 x 10^3) for $[Fe(bpyPY4)](OTf)_3 \cdot MeCN$. U(eq) is defined as one third of the trace of the orthogonalized Uij tensor.

	x	y	z	U(eq)
Fe(1)	8583(1)	814(1)	1343(1)	20(1)
S(1)	8949(1)	1289(1)	5970(1)	45(1)
S(2)	6248(1)	-974(1)	1985(1)	31(1)
S(3)	8727(1)	4232(1)	-1655(1)	44(1)
F(1)	8627(3)	-243(3)	5106(2)	83(1)

F(2)	7613(2)	723(2)	4755(2)	73(1)
F(3)	7938(3)	-154(3)	5742(2)	97(1)
F(4)	5233(3)	29(3)	2277(2)	89(1)
F(5)	6164(5)	847(2)	2190(3)	152(3)
F(6)	6457(2)	25(3)	3184(2)	73(1)
F(7)	9113(6)	3549(7)	-2667(5)	64(2)
F(7')	10285(4)	3935(6)	-1448(5)	88(2)
F(8)	7825(4)	3482(4)	-3041(3)	60(2)
F(8')	9381(8)	3108(10)	-2313(9)	126(5)
F(9)	8644(5)	2489(4)	-2180(4)	65(2)
F(9')	9741(6)	2768(6)	-1141(7)	123(4)
O(1)	9211(2)	1743(3)	5474(2)	60(1)
O(2)	9551(2)	751(3)	6597(2)	66(1)
O(3)	8406(3)	1888(4)	6141(2)	81(1)
O(4)	5715(3)	-868(3)	1192(2)	70(1)
O(5)	7111(3)	-860(4)	2203(3)	90(2)
O(6)	6103(2)	-1760(2)	2360(2)	52(1)
O(7)	8026(5)	3915(6)	-1487(4)	38(2)
O(7')	8121(5)	3642(7)	-1780(5)	60(2)
O(8)	9491(4)	4069(6)	-1075(4)	48(2)
O(8')	9216(5)	4592(6)	-840(4)	62(2)
O(9)	8678(16)	4959(17)	-2199(12)	64(5)
O(9')	8535(12)	5138(13)	-2043(10)	50(3)
N(1)	7450(2)	1206(2)	1113(2)	22(1)
N(2)	8268(2)	-523(2)	1366(2)	24(1)
N(3)	8054(2)	891(2)	229(2)	25(1)
N(4)	9039(2)	2013(2)	1218(2)	26(1)
N(5)	9715(2)	414(2)	1583(2)	26(1)
N(6)	8962(2)	981(2)	2447(2)	23(1)
N(7)	10531(5)	1613(5)	456(4)	102(2)
C(1)	7333(2)	2025(2)	1418(2)	27(1)
C(2)	6555(2)	2381(3)	1209(2)	31(1)
C(3)	5876(2)	1876(3)	683(2)	33(1)
C(4)	6000(2)	1032(3)	379(2)	31(1)
C(5)	6792(2)	708(2)	593(2)	23(1)
C(6)	6982(2)	-163(3)	206(2)	27(1)
C(7)	6179(2)	-654(3)	-368(2)	35(1)
C(8)	7554(2)	-872(3)	810(2)	27(1)
C(9)	7366(3)	-1836(3)	791(2)	37(1)
C(10)	7916(3)	-2433(3)	1358(3)	42(1)
C(11)	8632(3)	-2068(3)	1939(2)	36(1)
C(12)	8792(2)	-1109(3)	1928(2)	28(1)
C(13)	7409(2)	328(3)	-219(2)	28(1)
C(14)	7085(2)	366(3)	-1014(2)	33(1)
C(15)	7369(2)	1065(3)	-1335(2)	36(1)
C(16)	7912(2)	1757(3)	-879(2)	35(1)
C(17)	8239(2)	1663(3)	-83(2)	28(1)
C(18)	8771(2)	2343(3)	487(2)	30(1)
C(19)	9033(3)	3215(3)	349(3)	40(1)
C(20)	9610(3)	3718(3)	963(3)	43(1)
C(21)	9978(3)	3302(3)	1686(3)	36(1)
C(22)	9698(2)	2423(3)	1800(2)	29(1)
C(23)	10177(2)	1769(3)	2495(2)	29(1)
C(24)	10974(3)	2266(3)	3065(3)	41(1)
C(25)	10370(2)	873(3)	2145(2)	28(1)
C(26)	11165(2)	565(3)	2357(2)	39(1)
C(27)	11294(3)	-195(4)	1987(3)	49(1)
C(28)	10633(3)	-622(3)	1385(3)	45(1)
C(29)	9845(3)	-306(3)	1198(2)	34(1)
C(30)	9672(2)	1442(3)	2893(2)	26(1)
C(31)	9928(3)	1573(3)	3670(2)	37(1)
C(32)	9457(3)	1223(3)	3992(2)	39(1)
C(33)	8727(3)	744(3)	3529(2)	36(1)
C(34)	8500(2)	640(3)	2765(2)	28(1)
C(35)	8249(3)	368(4)	5374(3)	54(1)
C(36)	6024(4)	37(3)	2435(3)	51(1)
C(37)	8561(6)	3390(7)	-2439(5)	44(2)
C(37')	9587(7)	3479(8)	-1627(8)	68(3)
C(38)	10912(6)	2282(6)	474(5)	98(2)
C(39)	11323(6)	3206(7)	508(7)	133(4)

Table 3. Bond lengths [A] and angles [deg] for [Fe(bpyPY4)](OTf)$_3$•MeCN.

Fe(1)-N(4)	1.933(3)
Fe(1)-N(3)	1.942(3)
Fe(1)-N(2)	1.958(3)
Fe(1)-N(6)	1.960(3)
Fe(1)-N(5)	1.975(3)
Fe(1)-N(1)	1.976(3)
S(1)-O(1)	1.418(4)
S(1)-O(2)	1.425(3)
S(1)-O(3)	1.450(4)
S(1)-C(35)	1.807(5)
S(2)-O(4)	1.411(3)
S(2)-O(6)	1.413(3)
S(2)-O(5)	1.436(4)
S(2)-C(36)	1.808(5)
S(3)-O(7')	1.308(8)
S(3)-O(8)	1.349(6)
S(3)-O(9')	1.43(2)
S(3)-O(9)	1.45(2)
S(3)-O(8')	1.512(7)
S(3)-O(7)	1.527(8)
S(3)-C(37)	1.846(10)
S(3)-C(37')	1.868(12)
F(1)-C(35)	1.347(7)
F(2)-C(35)	1.327(5)
F(3)-C(35)	1.325(6)
F(4)-C(36)	1.328(7)
F(5)-C(36)	1.298(6)
F(6)-C(36)	1.309(6)
F(7)-C(37)	1.297(14)
F(7')-C(37')	1.317(12)
F(8)-C(37)	1.322(11)
F(8')-C(37')	1.325(17)
F(9)-C(37)	1.338(10)
F(9')-C(37')	1.313(14)
N(1)-C(1)	1.352(5)
N(1)-C(5)	1.353(4)
N(2)-C(8)	1.345(5)
N(2)-C(12)	1.350(5)
N(3)-C(13)	1.348(5)
N(3)-C(17)	1.358(5)
N(4)-C(22)	1.343(5)
N(4)-C(18)	1.364(5)
N(5)-C(29)	1.344(5)
N(5)-C(25)	1.353(5)
N(6)-C(30)	1.344(5)
N(6)-C(34)	1.348(5)
N(7)-C(38)	1.154(9)
C(1)-C(2)	1.375(5)
C(2)-C(3)	1.382(6)
C(3)-C(4)	1.385(6)
C(4)-C(5)	1.381(5)
C(5)-C(6)	1.555(5)
C(6)-C(8)	1.526(5)
C(6)-C(7)	1.535(5)
C(6)-C(13)	1.541(5)
C(8)-C(9)	1.384(5)
C(9)-C(10)	1.379(6)
C(10)-C(11)	1.372(6)
C(11)-C(12)	1.372(5)
C(13)-C(14)	1.390(5)
C(14)-C(15)	1.385(6)
C(15)-C(16)	1.376(6)
C(16)-C(17)	1.396(5)
C(17)-C(18)	1.445(5)
C(18)-C(19)	1.379(6)
C(19)-C(20)	1.370(6)
C(20)-C(21)	1.386(6)
C(21)-C(22)	1.386(5)
C(22)-C(23)	1.534(5)
C(23)-C(30)	1.527(5)
C(23)-C(24)	1.531(5)
C(23)-C(25)	1.543(5)
C(25)-C(26)	1.381(5)

C(26)-C(27)	1.366(6)
C(27)-C(28)	1.372(7)
C(28)-C(29)	1.381(6)
C(30)-C(31)	1.385(5)
C(31)-C(32)	1.371(6)
C(32)-C(33)	1.388(6)
C(33)-C(34)	1.365(5)
C(38)-C(39)	1.477(11)

N(4)-Fe(1)-N(3)	80.11(13)
N(4)-Fe(1)-N(2)	167.06(12)
N(3)-Fe(1)-N(2)	94.58(12)
N(4)-Fe(1)-N(6)	94.89(12)
N(3)-Fe(1)-N(6)	167.37(12)
N(2)-Fe(1)-N(6)	92.59(12)
N(4)-Fe(1)-N(5)	79.05(12)
N(3)-Fe(1)-N(5)	101.72(12)
N(2)-Fe(1)-N(5)	90.61(12)
N(6)-Fe(1)-N(5)	88.57(12)
N(4)-Fe(1)-N(1)	101.44(12)
N(3)-Fe(1)-N(1)	78.84(12)
N(2)-Fe(1)-N(1)	88.96(12)
N(6)-Fe(1)-N(1)	90.93(12)
N(5)-Fe(1)-N(1)	179.32(13)
O(1)-S(1)-O(2)	117.3(2)
O(1)-S(1)-O(3)	112.7(3)
O(2)-S(1)-O(3)	116.0(3)
O(1)-S(1)-C(35)	103.6(2)
O(2)-S(1)-C(35)	102.4(2)
O(3)-S(1)-C(35)	101.9(3)
O(4)-S(2)-O(6)	117.1(2)
O(4)-S(2)-O(5)	114.7(3)
O(6)-S(2)-O(5)	112.1(3)
O(4)-S(2)-C(36)	105.1(2)
O(6)-S(2)-C(36)	102.2(2)
O(5)-S(2)-C(36)	103.5(3)
O(8)-S(3)-O(9')	120.0(8)
O(7')-S(3)-O(9)	123.1(11)
O(7')-S(3)-O(8')	116.2(5)
O(9)-S(3)-O(8')	110.6(9)
O(8)-S(3)-O(7)	114.2(4)
O(9')-S(3)-O(7)	110.3(7)
O(8)-S(3)-C(37)	107.6(5)
O(9')-S(3)-C(37)	102.3(6)
O(7)-S(3)-C(37)	99.6(4)
O(7')-S(3)-C(37')	106.2(6)
O(9)-S(3)-C(37')	100.3(9)
O(8')-S(3)-C(37')	94.6(6)
C(1)-N(1)-C(5)	120.0(3)
C(1)-N(1)-Fe(1)	119.7(2)
C(5)-N(1)-Fe(1)	120.0(2)
C(8)-N(2)-C(12)	119.8(3)
C(8)-N(2)-Fe(1)	120.7(2)
C(12)-N(2)-Fe(1)	119.4(2)
C(13)-N(3)-C(17)	119.6(3)
C(13)-N(3)-Fe(1)	122.0(2)
C(17)-N(3)-Fe(1)	117.0(2)
C(22)-N(4)-C(18)	119.5(3)
C(22)-N(4)-Fe(1)	122.0(2)
C(18)-N(4)-Fe(1)	117.4(2)
C(29)-N(5)-C(25)	119.5(3)
C(29)-N(5)-Fe(1)	121.0(3)
C(25)-N(5)-Fe(1)	119.5(2)
C(30)-N(6)-C(34)	119.3(3)
C(30)-N(6)-Fe(1)	121.1(2)
C(34)-N(6)-Fe(1)	119.6(2)
N(1)-C(1)-C(2)	121.8(3)
C(1)-C(2)-C(3)	118.9(4)
C(2)-C(3)-C(4)	119.1(4)
C(5)-C(4)-C(3)	120.3(4)
N(1)-C(5)-C(4)	120.0(3)
N(1)-C(5)-C(6)	116.6(3)
C(4)-C(5)-C(6)	123.1(3)
C(8)-C(6)-C(7)	110.9(3)
C(8)-C(6)-C(13)	111.9(3)

C(7)-C(6)-C(13)	110.5(3)
C(8)-C(6)-C(5)	110.8(3)
C(7)-C(6)-C(5)	110.8(3)
C(13)-C(6)-C(5)	101.6(3)
N(2)-C(8)-C(9)	120.6(3)
N(2)-C(8)-C(6)	116.9(3)
C(9)-C(8)-C(6)	122.5(3)
C(10)-C(9)-C(8)	119.0(4)
C(11)-C(10)-C(9)	120.2(4)
C(10)-C(11)-C(12)	118.4(4)
N(2)-C(12)-C(11)	121.9(3)
N(3)-C(13)-C(14)	119.8(4)
N(3)-C(13)-C(6)	114.4(3)
C(14)-C(13)-C(6)	124.6(3)
C(15)-C(14)-C(13)	119.0(4)
C(16)-C(15)-C(14)	120.4(4)
C(15)-C(16)-C(17)	117.9(4)
N(3)-C(17)-C(16)	120.8(4)
N(3)-C(17)-C(18)	113.0(3)
C(16)-C(17)-C(18)	126.2(4)
N(4)-C(18)-C(19)	121.1(4)
N(4)-C(18)-C(17)	112.2(3)
C(19)-C(18)-C(17)	126.6(4)
C(20)-C(19)-C(18)	118.3(4)
C(19)-C(20)-C(21)	119.8(4)
C(20)-C(21)-C(22)	119.7(4)
N(4)-C(22)-C(21)	119.5(4)
N(4)-C(22)-C(23)	114.8(3)
C(21)-C(22)-C(23)	124.6(4)
C(30)-C(23)-C(24)	110.9(3)
C(30)-C(23)-C(22)	113.7(3)
C(24)-C(23)-C(22)	109.7(3)
C(30)-C(23)-C(25)	107.6(3)
C(24)-C(23)-C(25)	110.9(3)
C(22)-C(23)-C(25)	103.8(3)
N(5)-C(25)-C(26)	120.4(4)
N(5)-C(25)-C(23)	116.6(3)
C(26)-C(25)-C(23)	122.9(3)
C(27)-C(26)-C(25)	119.9(4)
C(26)-C(27)-C(28)	119.7(4)
C(27)-C(28)-C(29)	118.8(4)
N(5)-C(29)-C(28)	121.5(4)
N(6)-C(30)-C(31)	120.7(3)
N(6)-C(30)-C(23)	116.0(3)
C(31)-C(30)-C(23)	123.3(3)
C(32)-C(31)-C(30)	119.8(4)
C(31)-C(32)-C(33)	119.1(4)
C(34)-C(33)-C(32)	118.8(4)
N(6)-C(34)-C(33)	122.3(4)
F(3)-C(35)-F(2)	106.9(5)
F(3)-C(35)-F(1)	106.9(5)
F(2)-C(35)-F(1)	105.5(4)
F(3)-C(35)-S(1)	113.0(4)
F(2)-C(35)-S(1)	112.6(4)
F(1)-C(35)-S(1)	111.5(4)
F(5)-C(36)-F(6)	107.9(5)
F(5)-C(36)-F(4)	107.5(5)
F(6)-C(36)-F(4)	106.6(4)
F(5)-C(36)-S(2)	111.8(4)
F(6)-C(36)-S(2)	112.5(4)
F(4)-C(36)-S(2)	110.3(4)
F(7)-C(37)-F(8)	107.8(8)
F(7)-C(37)-F(9)	108.8(9)
F(8)-C(37)-F(9)	108.6(8)
F(7)-C(37)-S(3)	109.0(8)
F(8)-C(37)-S(3)	112.9(7)
F(9)-C(37)-S(3)	109.6(6)
F(9')-C(37')-F(7')	108.5(11)
F(9')-C(37')-F(8')	108.0(12)
F(7')-C(37')-F(8')	104.1(11)
F(9')-C(37')-S(3)	109.8(9)
F(7')-C(37')-S(3)	115.6(8)
F(8')-C(37')-S(3)	110.6(10)
N(7)-C(38)-C(39)	173.1(10)

Symmetry transformations used to generate equivalent atoms:

Table 4. Anisotropic displacement parameters (A^2 x 10^3) for [Fe(bpyPY4)](OTf)$_3$•MeCN. The anisotropic displacement factor exponent takes the form:
-2 pi^2 [h^2 a*^2 U11 + ... + 2 h k a* b* U12]

	U11	U22	U33	U23	U13	U12
Fe(1)	19(1)	19(1)	21(1)	0(1)	8(1)	0(1)
S(1)	46(1)	50(1)	28(1)	2(1)	8(1)	2(1)
S(2)	38(1)	27(1)	26(1)	-1(1)	12(1)	-11(1)
S(3)	53(1)	42(1)	38(1)	9(1)	22(1)	-2(1)
F(1)	101(3)	59(2)	64(2)	-10(2)	17(2)	10(2)
F(2)	64(2)	78(2)	41(2)	8(2)	-6(1)	-3(2)
F(3)	96(3)	118(3)	56(2)	17(2)	17(2)	-51(2)
F(4)	96(3)	92(3)	64(2)	-1(2)	24(2)	59(2)
F(5)	384(9)	20(2)	133(4)	-15(2)	188(5)	-29(3)
F(6)	93(2)	83(2)	40(2)	-28(2)	27(2)	-19(2)
F(7)	75(6)	69(6)	69(5)	4(4)	50(5)	-2(4)
F(7')	72(5)	88(5)	125(6)	10(4)	63(5)	-8(4)
F(8)	70(4)	59(4)	35(3)	-4(3)	11(3)	-22(3)
F(8')	108(9)	133(11)	174(14)	-80(9)	97(10)	-36(8)
F(9)	113(6)	29(3)	63(4)	6(3)	51(4)	2(3)
F(9')	112(7)	63(5)	214(11)	52(6)	93(7)	20(4)
O(1)	64(2)	59(2)	55(2)	8(2)	26(2)	-4(2)
O(2)	51(2)	73(3)	42(2)	14(2)	-6(2)	-1(2)
O(3)	70(3)	101(3)	65(2)	-30(2)	26(2)	10(2)
O(4)	103(3)	55(2)	25(2)	2(2)	6(2)	33(2)
O(5)	65(3)	122(4)	106(3)	-63(3)	60(3)	-57(3)
O(6)	75(2)	32(2)	66(2)	15(2)	46(2)	9(2)
O(7)	28(3)	50(5)	32(4)	12(3)	12(3)	2(3)
O(7')	50(5)	67(6)	62(6)	7(4)	24(4)	-16(4)
O(8)	31(3)	58(5)	45(4)	8(4)	9(3)	-6(3)
O(8')	81(5)	66(5)	44(4)	-2(3)	34(4)	-25(4)
O(9)	78(10)	67(11)	42(8)	12(7)	24(5)	-14(8)
O(9')	61(7)	37(5)	38(7)	3(4)	11(5)	-16(5)
N(1)	22(1)	21(1)	24(1)	3(1)	11(1)	1(1)
N(2)	23(2)	21(1)	23(2)	-2(1)	7(1)	1(1)
N(3)	23(2)	27(2)	25(2)	1(1)	10(1)	6(1)
N(4)	27(2)	22(2)	31(2)	0(1)	16(1)	2(1)
N(5)	22(2)	25(2)	29(2)	-1(1)	11(1)	2(1)
N(6)	21(1)	21(2)	23(1)	-2(1)	9(1)	-2(1)
N(7)	112(5)	86(4)	92(4)	-9(4)	33(4)	-16(4)
C(1)	32(2)	20(2)	31(2)	0(1)	16(2)	-2(1)
C(2)	36(2)	23(2)	42(2)	4(2)	25(2)	5(2)
C(3)	29(2)	29(2)	46(2)	11(2)	21(2)	7(2)
C(4)	24(2)	31(2)	35(2)	5(2)	11(2)	1(2)
C(5)	23(2)	21(2)	24(2)	4(1)	10(1)	-1(1)
C(6)	23(2)	27(2)	24(2)	-3(1)	5(2)	0(1)
C(7)	26(2)	35(2)	31(2)	-6(2)	2(2)	-4(2)
C(8)	27(2)	22(2)	27(2)	-5(1)	9(2)	0(1)
C(9)	35(2)	24(2)	40(2)	-6(2)	9(2)	-5(2)
C(10)	45(2)	20(2)	52(3)	-3(2)	15(2)	-4(2)
C(11)	36(2)	26(2)	38(2)	4(2)	10(2)	5(2)
C(12)	25(2)	25(2)	27(2)	-2(2)	7(2)	2(1)
C(13)	25(2)	28(2)	27(2)	-4(2)	10(2)	7(1)
C(14)	28(2)	38(2)	26(2)	-4(2)	8(2)	9(2)
C(15)	34(2)	50(2)	23(2)	4(2)	12(2)	17(2)
C(16)	35(2)	42(2)	32(2)	9(2)	20(2)	12(2)
C(17)	25(2)	32(2)	31(2)	3(2)	16(2)	7(2)
C(18)	31(2)	30(2)	34(2)	6(2)	21(2)	6(2)
C(19)	48(3)	35(2)	47(2)	10(2)	31(2)	0(2)
C(20)	51(3)	27(2)	64(3)	3(2)	38(2)	-5(2)
C(21)	37(2)	28(2)	50(2)	-5(2)	25(2)	-7(2)
C(22)	31(2)	25(2)	39(2)	-6(2)	23(2)	-3(2)
C(23)	24(2)	30(2)	32(2)	-5(2)	10(2)	-6(2)
C(24)	30(2)	46(3)	42(2)	-12(2)	12(2)	-14(2)
C(25)	23(2)	31(2)	30(2)	0(2)	13(2)	-1(2)
C(26)	23(2)	54(3)	36(2)	-3(2)	10(2)	1(2)

C(27)	29(2)	64(3)	54(3)	-1(2)	20(2)	14(2)
C(28)	38(2)	49(3)	51(3)	-7(2)	22(2)	13(2)
C(29)	34(2)	30(2)	37(2)	-4(2)	15(2)	4(2)
C(30)	26(2)	22(2)	29(2)	-3(1)	12(2)	0(1)
C(31)	36(2)	36(2)	31(2)	-8(2)	10(2)	-5(2)
C(32)	45(2)	44(2)	27(2)	-5(2)	15(2)	1(2)
C(33)	40(2)	41(2)	32(2)	0(2)	21(2)	0(2)
C(34)	26(2)	30(2)	29(2)	1(2)	14(2)	0(2)
C(35)	56(3)	58(3)	34(2)	8(2)	8(2)	-1(2)
C(36)	83(4)	31(2)	42(3)	-1(2)	31(3)	2(2)
C(37)	50(6)	39(5)	42(5)	10(4)	21(5)	-6(4)
C(37')	60(7)	54(7)	96(9)	-8(6)	41(7)	-15(5)
C(38)	119(7)	81(5)	108(6)	-29(4)	63(5)	-32(5)
C(39)	120(7)	104(7)	218(12)	-17(7)	115(8)	-26(6)

Table 5. Hydrogen coordinates (x 10^4) and isotropic displacement parameters (A^2 x 10^3) for [Fe(bpyPY4)](OTf)$_3$•MeCN.

	x	y	z	U(eq)
H(1)	7801	2363	1786	32
H(2)	6485	2963	1423	37
H(3)	5332	2105	532	40
H(4)	5538	675	22	37
H(7A)	5822	-186	-749	52
H(7B)	6310	-1175	-628	52
H(7C)	5892	-916	-93	52
H(9)	6865	-2084	394	44
H(10)	7799	-3098	1347	50
H(11)	9007	-2471	2339	43
H(12)	9286	-850	2327	33
H(14)	6676	-80	-1332	39
H(15)	7188	1067	-1873	43
H(16)	8059	2282	-1098	42
H(19)	8819	3461	-158	47
H(20)	9757	4350	893	51
H(21)	10421	3617	2103	44
H(24A)	11288	2470	2798	62
H(24B)	10837	2828	3283	62
H(24C)	11309	1820	3479	62
H(26)	11622	880	2760	47
H(27)	11838	-428	2145	59
H(28)	10716	-1125	1102	54
H(29)	9385	-605	787	41
H(31)	10429	1904	3979	44
H(32)	9629	1307	4525	47
H(33)	8392	493	3739	43
H(34)	7998	315	2447	34
H(39A)	10906	3686	206	199
H(39B)	11711	3126	296	199
H(39C)	11624	3419	1043	199